Accepted to ApJ, 2012 September 12
Preprint typeset using LaTeX style emulateapj v. 5/2/11

THE BIZARRE CHEMICAL INVENTORY OF NGC 2419, AN EXTREME OUTER HALO GLOBULAR CLUSTER[1]

Judith G. Cohen[2] and Evan N. Kirby[2,3]

Accepted to ApJ, 2012 September 12

ABSTRACT

We present new Keck/HIRES observations of six red giants in the globular cluster NGC 2419. Although the cluster is among the most distant and most luminous in the Milky Way, it was considered chemically ordinary until very recently. Our previous work showed that the near-infrared Ca II triplet line strength varied more than expected for a chemically homogeneous cluster, and that at least one star had unusual abundances of Mg and K. Here, we confirm that NGC 2419 harbors a population of stars, comprising about one third of its mass, that is depleted in Mg by a factor of 8 and enhanced in K by a factor of 6 with respect to the Mg-normal population. Although the majority, Mg-normal population appears to have a chemical abundance pattern indistinguishable from ordinary, inner halo globular clusters, the Mg-poor population exhibits dispersions of several elements. The abundances of K and Sc are strongly anti-correlated with Mg, and some other elements (Si and Ca among others) are weakly anti-correlated with Mg. These abundance patterns suggest that the different populations of NGC 2419 sample the ejecta of diverse supernovae in addition to AGB ejecta. However, the abundances of Fe-peak elements except Sc show no star-to-star variation. We find no nucleosynthetic source that satisfactorily explains all of the abundance variations in this cluster. Because NGC 2419 appears like no other globular cluster, we reiterate our previous suggestion that it is not a globular cluster at all, but rather the core of an accreted dwarf galaxy.

Subject headings: Galaxy: globular clusters: individual (NGC 2419), Galaxy: formation, Galaxy: halo

1. INTRODUCTION

NGC 2419 is one of the most unusual globular clusters (GCs) belonging to the Milky Way (MW). It resides in the MW's outer halo (Harris et al. 1997, 90 kpc from the Galactic center). It is notable not just for its distance but also its luminosity. M54, the core of the Sagittarius dwarf galaxy (Ibata et al. 1995), is the only GC more luminous than NGC 2419.

The first *Hubble Space Telescope* (HST) photometry (Harris et al. 1997) of NGC 2419 showed that the cluster is as old as the inner halo cluster M92. In other words, NGC 2419 is about as old as the Universe. Like many GCs, NGC 2419 is a "second parameter" cluster, with an extended blue horizontal branch (HB). di Criscienzo et al. (2011) attributed the HB morphology and the color dispersion at the base of the red giant branch (RGB) to a different helium abundance between the first and second generations of stars, a popular explanation for the second parameter in GCs (D'Antona et al. 2002).

The distance and photometric properties of the cluster alone are not extremely unusual, but the chemical properties of the cluster are. Early spectroscopy (Suntzeff et al. 1988) did not reveal any unusual abundance patterns in the cluster. In particular, the iron abundance appeared invariable from star to star. Much more recently, medium-resolution (Keck/DEIMOS) spectroscopy by Cohen et al. (2010, hereafter C10) showed that the strength of the infrared calcium triplet (CaT) varies from star to star, even at fixed stellar luminosity. Ibata et al. (2011) confirmed this star-to-star variation with independent DEIMOS spectroscopy. C10 attributed this variation to a range of calcium abundance[4] (σ([Ca/H]) ~ 0.2) in the cluster.

Later high-resolution (Keck/HIRES) spectroscopy by Cohen, Huang & Kirby (2011, hereafter C11) revealed an even more complex abundance distribution. Six of seven stars appeared identical to stars in "normal" GCs, such as those found in the inner halo of the MW. However, star S1131 had [K/Fe] = 1.1 (very high for a GC) and [Mg/Fe] = -0.5 (very low for a GC). Such a low value of [Mg/Fe] can be found only in the most metal-rich stars in dwarf spheroidal galaxies (Letarte et al. 2010; Cohen & Huang 2010; Kirby et al. 2011). It is never found in stars with the metallicity of NGC 2419 ([Fe/H] = -2.1). Furthermore, low values of [Mg/Fe] in halo and dwarf galaxy stars are always accompanied by low abundances of other α elements, such as Si and Ca. Star S1131 exhibits enhanced ratios of [Si/Fe] and [Ca/Fe], typical for a normal GC star.

C11's HIRES sample provided no compelling evidence for a variation in elements heavier than potassium, such as Fe and other iron-peak elements. Even Ca, in which a dispersion was detected with DEIMOS, appeared to be constant across the stars from HIRES data. Importantly, the DEIMOS analysis was based on ionized Ca lines whereas the HIRES analysis was based on neutral

[1] Based in part on observations obtained at the W.M. Keck Observatory, which is operated jointly by the California Institute of Technology, the University of California, and the National Aeronautics and Space Administration.

[2] Palomar Observatory, Mail Stop 249-17, California Institute of Technology, Pasadena, Ca., 91125, jlc(enk)@astro.caltech.edu

[3] Hubble Fellow

[4] The standard nomenclature is adopted; the abundance of element X is given by $\epsilon(X) = N(X)/N(H)$ on a scale where $N(H) = 10^{12}$ H atoms. Then [X/H] = $\log_{10}$[N(X)/N(H)] − $\log_{10}$[N(X)/N(H)]$_\odot$, and similarly for [X/Fe].

Ca lines.

The HIRES sample of C11 included only one of the Ca-rich stars identified by C10. In fact, that single star was S1131, the one with unusual magnesium and potassium abundances. The peculiarity of this star with a strong CaT demanded that we observe additional stars from the DEIMOS sample with large CaT line strengths. In this article, we expand C11's sample of HIRES spectra in NGC 2419, focusing in particular on the stars with strong CaT lines.

2. OBSERVATIONS AND ABUNDANCE ANALYSIS PROCEDURES

In an effort to overcome some of the limitations of and concerns arising from our previous work in NGC 2419, we obtained HIRES-R (Vogt et al. 1994) spectra of an additional 6 stars in this GC during a 4 night run which began 2012 Jan 29. The spectrograph configuration was identical to that we used in our 2008 and 2010 observations of NGC 2419 red giants. Most of the new stars were chosen to probe the Ca-rich distribution of the DEIMOS measurements of the Ca triplet, with preference given to those stars for which we had already obtained low signal-to-noise ratio (S/N) HIRES spectra that suggested, based on our measured radial velocities, that the stars were cluster members. These stars are faint ($17.5 < V < 17.9$) for high-resolution spectroscopy, and the exposure times ranged from 2.5 hours for the brightest star to 4 hours for the faintest star. All of the nights were clear, and two had excellent seeing.

The total sample of 13 stars for which we obtained reasonably good HIRES spectra is given in Table 1. Fig. 1 shows a comparison of the location of the sample stars on the observed V, $V-I$ plane using optical photometry from Stetson (2005) and the V, $V-J$ plane, where J is from 2MASS (Skrutskie et al. 2006; Cutri et al. 2003). Isochrones from the Y^2 grid (Yi et al. 2003) for an age of 12 Gyr with [Fe/H] $= -2.20$ dex (solid line) and [Fe/H] $= -1.90$ dex (dotted line), both with [α/Fe] $= +0.30$ dex, are indicated. We adopted the same distance and reddening as was used in C11. In our earlier work (C10), the membership of star S1673 in NGC 2419 was considered possible but not definite. This is because, as is seen in Fig 1, this star lies to the blue of the main cluster RGB in a V, $V-I$ CMD. Although its v_r is consistent with cluster membership, we decided to be cautious and not consider it a confirmed member at that time. However, on the basis of its abundances, discussed below, we now consider S1673 to be a definite member of this GC. It may be, as C10 speculated, an AGB rather than a RGB star.

Fig. 2 shows a histogram of Ca(CaT), the Ca abundance inferred from our initial moderate resolution study (C10) based on the CaT line strength measured with DEIMOS on Keck II, with the HIRES sample indicated. Our HIRES sample now includes giants spanning almost the entire range of Ca(CaT) abundances for NGC 2419 luminous giants. While there are a few stars in our DEIMOS sample with even higher Ca(CaT), they are not in our HIRES sample as they are all fainter than $V = 17.7$.

The measurement of equivalent widths, whose values are given in Tables 2 and 3, and the abundance analyses were carried out in a manner identical to our previous

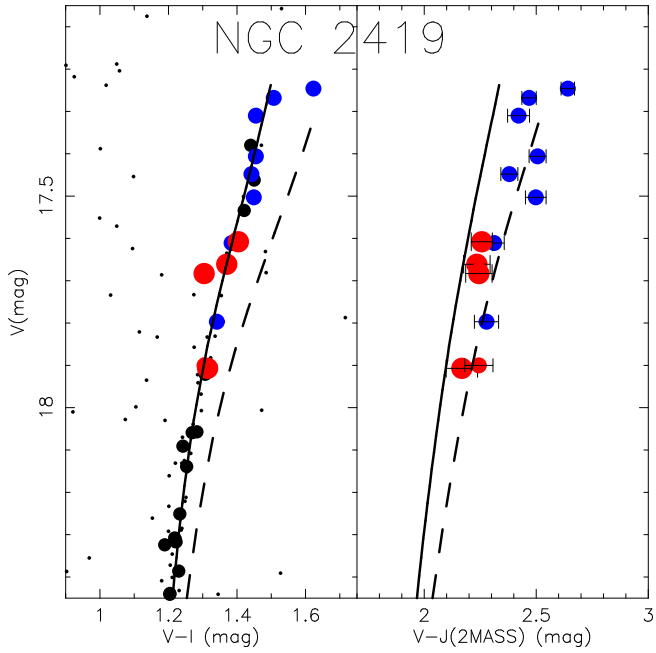

Figure 1. The V, $V-I$ (left panel) and V, $V-J$ (right panel) CMDs are shown for NGC 2419 with optical photometry from Stetson (2005) and J photometry from 2MASS. The red circles denote stars with [Mg/Fe] < 0, while the blue circles represent stars with [Mg/Fe] > 0 dex. The larger symbols denote stars whose DEIMOS spectra have near-IR Ca triplet lines implying [Ca/H] > -1.8. Two 12 Gyr, α-enhanced isochrones from Yi et al. (2003) are shown: [Fe/H] $= -2.2$ (solid line) and [Fe/H] $= -1.9$ (dashed line). The smallest black points, seen only in the left panel, are the photometric sample of Stetson (2005). The somewhat larger black points (also shown only in the left panel) are the Keck/DEIMOS sample of C10.

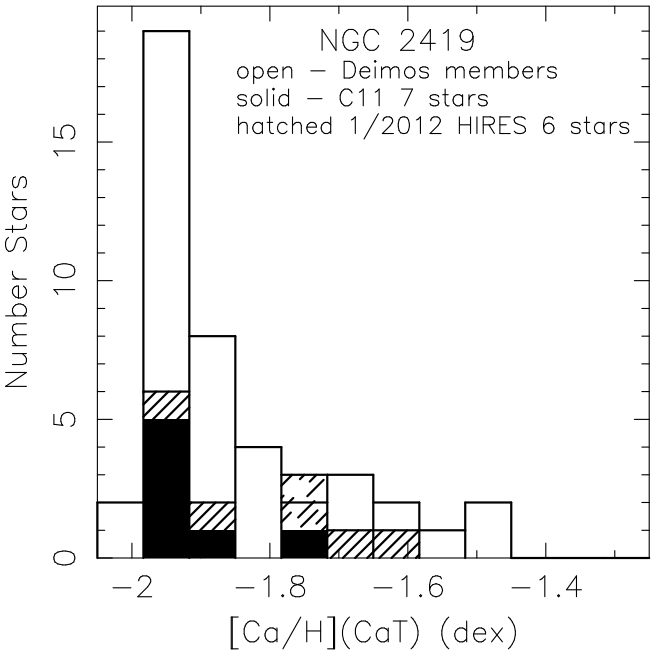

Figure 2. A histogram of [Ca/H] as inferred from the near-IR Ca II triplet line strengths in the DEIMOS moderate resolution spectra of C10 is shown for the sample of 43 definite members of NGC 2419 isolated in that paper. The sample from C11 of 7 RGB stars in this GC with HIRES spectra is shown by the solid fill. The 6 additional NGC 2419 stars presented here are indicated by the hatched areas.

Table 1
Data for Red Giant Members of NGC 2419 With Keck/HIRES Spectra

Name[a]	V[a] (mag)	$T_{\rm eff}$, log(g),v_t [b] (K, dex, km s^{-1})	Exp. Time (sec)	S/N[c]	v_r (km s^{-1})
New Stars					
Stet 406	17.80	4448, 0.95	14400	95	−20.3
Stet 458	17.90	4480, 1.02	10800	85	−17.9
Stet 1004	17.91	4482, 1.02	14400	80	−23.5
Stet 1065	17.66	4455, 0.88	10800	80	−22.7
Stet 1166	17.50	4350, 0.89	9000	82	−21.3
Stet 1673	17.68	4409, 0.88	10800	95	−24.6
From C11					
Stet 223[d]	17.25	4265, 0.61	8400	> 100	−22.4
Stet 810	17.31	4316, 0.65	7200	> 100	−22.6
Stet 973[e]	17.45	4325, 0.74	3200	39	−21.9
Stet 1131	17.61	4382, 0.84	9000	95	−16.8
Stet 1209[f]	17.41	4317, 0.71	7200	93	−19.0
Stet 1305[g]	17.61	4385, 0.84	3000	52	−16.8
Stet 1814[h]	17.27	4472, 0.62	5400	90	−26.1

[a] Star IDs and V magnitudes are from the online version of the database of Stetson (2005).
[b] These values, adopted for the abundance analysis, are based only on the V mag and an appropriate isochrone.
[c] SNR per spectral resolution element in the continuum at 5500 Å.
[d] Stetson 223 = Suntzeff 1.
[e] Stetson 973 = Suntzeff 15.
[f] Stetson 1209 = Suntzeff 16.
[g] Stetson 1305 = RH 10 (private communication from M. Shetrone), previously observed by Shetrone, Côté & Sargent (2001).
[h] Stetson 1814 = Suntzeff 14.

work. C11 described those procedures in detail. W_λ for the 7 stars from C11 are also listed there as a number of lines were added since 2011. Hyperfine structure corrections have been made following C11. No non-LTE corrections were made because the Al abundances were calculated not from the 3950 Å resonance doublet but from the weak 6696, 6698 Å doublet, which has no strong non-LTE correction (see Baumüller & Gehren 1997). The magnitudes of the expected non-LTE corrections for some other key elements are discussed in §4. Because these are rather faint metal-poor giants, we included the strong Mg triplet lines and sometimes the Na D lines in the analysis in order to get a reasonable number of lines for these key elements. We provide two measurements of abundance for these two elements: one with and one without these very strong lines.

We made two important updates to our procedures described in C11. We are now using the 2010 version of MOOG (Sneden 1973) updated by J. Sobeck (Sobeck et al. 2011). The new version contains a better treatment of coherent, isotropic scattering, which in the 2002 version is treated as pure absorption. This could be important for our NGC 2419 sample primarily because these are cool luminous RGB stars. But since [Fe/H] for NGC 2419 is about −2.1 dex, the importance of Rayleigh scattering as an opacity source is not as large as it would be for even more metal-poor stars. Furthermore, we did not consider lines blueward of 4100 Å because the spectral S/N is too low at those wavelengths. We focused on the part of the spectra $\lambda > 4500$ Å, where S/N is higher, unless an element has no or very few lines beyond 4500 Å. Thus, for our sample, the use of the 2010 version of MOOG does not introduce noticeable changes compared to the 2002 version.

The second major change change we made involves the determination of stellar parameters. Fig. 1 shows the V, $V-I$ and V, $V-J$ CMDs for our HIRES sample in NGC 2419, with two metal-poor, α-enhanced, 12 Gyr Yonsei-Yale isochrones (Yi et al. 2003) superposed. We set the stellar parameters $T_{\rm eff}$ and log(g) by assuming the stars lie on an isochrone halfway between the two shown in Fig. 1. We did not use the colors at all, just the V magnitude, to set $T_{\rm eff}$ and log(g). When looking for small abundance variations, the choice of stellar parameters is critical, as discussed by C11. Rather than relying on colors, which for such faint stars have non-trivial uncertainties, particularly those from 2MASS, we decided to force the stars to lie on an isochrone with just the V measurements taken from Stetson (2005), whose uncertainties are quite small ($\leq$0.015 mag), over a total range spanned by our sample of 17.25 to 17.91 mag. The range in $V-I$ spanned by our sample is only 0.32 mag, less than half of that of V and with somewhat larger uncertainties. The range in $V-J$ is 0.47 mag, but the uncertainties are much larger due to the limited depth of 2MASS. If the stars really do lie along a single isochrone, as would be the case if NGC 2419 is actually a chemically homogeneous old GC, using just V will give a very accurate relative $T_{\rm eff}$ determination for each star. Even if a slightly inappropriate isochrone is used, the relative differences in $T_{\rm eff}$ for members along the upper RGB of the stellar population will be highly accurate. Fig. 3 shows the dependence of [Fe I/H], [Fe II/H] and the difference of the two as a function of V (our proxy for $T_{\rm eff}$), as well as the same for Ti. The behavior of these key diagnostics serves to demonstrate that our detailed abundance

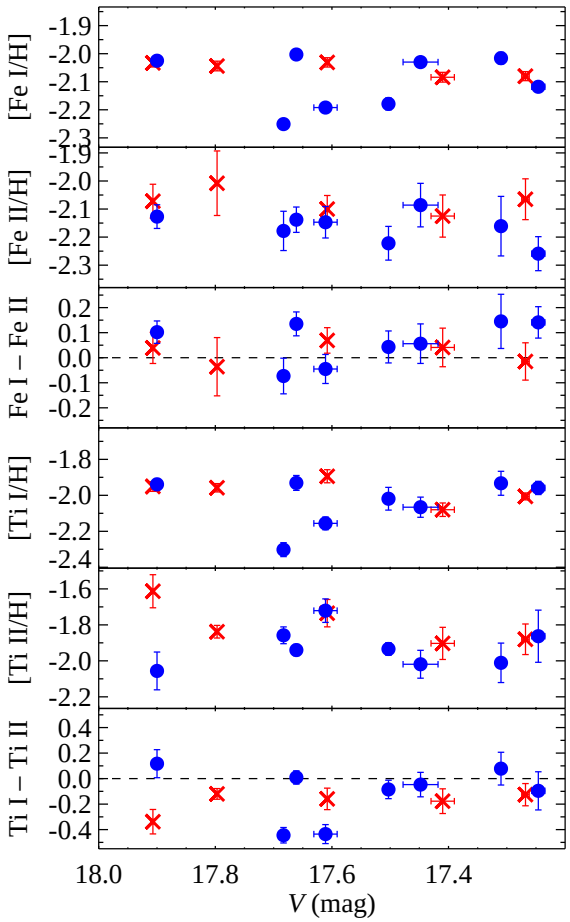

Figure 3. Diagnostic abundance ratios for two stages of ionization of Fe and of Ti are shown as a function of V magnitude for our sample of 13 luminous RGB stars in NGC 2419. Red crosses and blue points denote Mg-poor and Mg-rich giants respectively.

analyses are valid.

3. THE CHEMICAL INVENTORY OF THE NGC 2419 GIANTS

Our detailed abundance analysis for 13 luminous red giants in NGC 2419 yielded the results given in Tables 4 and 5. The Mg abundances are listed with the two Mg triplet lines both included and excluded to illustrate that the result is identical to within the errors even when the strong Mg triplet lines are included. The abundance analyses for the 7 stars from C11 were redone, resulting only in small differences. The present results supersede those of C11. Tables of uncertainties for the absolute abundances and the abundance ratios were given in C11.

One star, S1673, appears to be significantly bluer than the RGB of NGC 2419 in the V, $V-I$ CMD, but less discrepant in the V, $V-J$ CMD. It may be an AGB star. We carried out an abundance analysis for this star based solely on its V magnitude (i.e., assuming that it lies on the normal RGB) and also one assuming that it is 100 K hotter than the RGB and with a slightly lower $\log(g)$ corresponding to a mass of 0.6 $M_{\odot}$ instead of 0.8 $M_{\odot}$ (i.e., on the AGB). Both sets of results are presented in Table 4.

Our detailed abundance analysis shows that NGC 2419 contains two groups of stars. The first, containing 8 of the 13 stars, represents a normal α-rich population typical of GC (and inner halo) stars. This is the population that dominated the sample of C11, where it was shown that they are essentially identical in chemical inventory to the stars in the much nearer, inner halo cluster NGC 7099 with similar metallicity.

However, the second population found here is very strange. It shows extreme depletions of Mg, with [Mg/Fe] ranging widely from -0.2 to -0.7 dex, accompanied by large enhancements in K of $\sim$0.7 dex above those of the "normal" NGC 2419 giants. The Mg-poor group contains the same 5 stars shown in Fig. 2 to have stronger near-IR Ca triplet lines from the study of C10. The fraction of stars in the high tail of the Ca(CaT) distribution (Ca/H] > -1.85) from the larger DEIMOS sample of C10 is 34%; the fraction of peculiar Mg-poor stars in the smaller HIRES sample is comparable (38%).

Table 6 gives the mean abundances for each of the two groups. A number of smaller anomalies are apparent from this table, and are also visible in Fig 4. We see that the Mg-poor group of luminous RGB stars in NGC 2419 has slightly higher [Si/Fe], [Sc/Fe], and [Ca/Fe] than does the group of normal giants. However the majority of the elements probed have identical abundances with relatively small dispersions in the two groups of NGC 2419 stars. This specifically includes Fe.

Figs. 5 to 9 show sums of the spectra of the Mg-poor RGB stars in NGC 2419 and those of the Mg-normal stars to illustrate the contrast between the two groups. The Mg-normal star S223, the brightest and reddest cluster member, has been omitted from all the sums. S223 has broader metal lines and extremely strong Hα emission. Note that the mean $T_{\rm eff}$ of the Mg-poor stars is $\sim$100 K hotter than that of the Mg-normal stars (see Fig. 1). The specific features shown are (5) a set of Fe I lines, with one Fe II line, to illustrate that there is no evidence of a variation in Fe abundance, (6) the region of the 5528 Å Mg I line which includes a Sc II line, (7) the Na doublet at 5685 Å, to show that the Na abundance is low in both groups, (8) an even weaker Na doublet near 6160 Å, and (9) a set of Ca I lines near 6165 Å. The last of these figures shows that the Ca I lines in the Mg-poor group are only slightly stronger than those in the Mg-normal group of NGC 2419 giants. If the differences in line strength were due to temperature alone, the lines would be weaker. Hence, there is a difference in the average Ca abundance between the two groups.

The extremely low [Mg/Fe] abundances we have determined for the Mg-poor group of 5 giants in NGC 2419 are very unusual. Such low values of [Mg/Fe] can be found only in the most metal-rich stars in dwarf spheroidal galaxies (Letarte et al. 2010; Cohen & Huang 2010; Kirby et al. 2011). It is never found in stars with the metallicity of NGC 2419 ([Fe/H] $= -2.1$). For example, the 122 stars of the 0Z project have a median [Fe/H] of -2.9 dex, and 10% of the sample has [Fe/H] > -2.3 dex. The lowest value of [Mg/Fe] in this sample of Galactic halo field EMP candidates is -0.23 dex, with normal [K/Fe]. Note that only three of 122 stars in their sample have [Mg/Fe] < 0 (Cohen et al., in preparation). Furthermore, low values of [Mg/Fe] in halo and dwarf

Table 6
Mean Absolute Abundances for the Two Groups of Red Giant Members of NGC 2419 With Keck/HIRES Spectra

	Mg-rich[a]			Mg-poor[b]		
Species	log[ϵ(X)]	σ	N(stars)	log[ϵ(X)]	σ	N(stars)
C(CH)	5.75	0.19	7	5.71	0.22	5
NaI	4.31	0.29	8	4.35	0.13	5
MgI	5.78	0.14	8	4.92	0.30	5
MgI[c]	5.74	0.14	5	4.80	0.39	3
AlI	4.94	0.25	4	4.93	0.11	4[d]
SiI	5.81	0.07	6	6.05	0.10	5
KI	3.46	0.16	8	4.26	0.13	5
CaI[e]	4.40	0.09	8	4.58	0.03	5
CaT[f]	4.39	0.03	8	4.66	0.04	5
ScII	1.10	0.04	8	1.55	0.16	5
TiI	2.95	0.13	8	2.97	0.11	5
TiII	3.01	0.14	8	3.12	0.12	5
TiII[g]	3.05	0.10	8	3.21	0.12	5
VI	1.91	0.15	8	2.03	0.16	5
CrI	3.21	0.14	8	3.29	0.11	5
MnI	2.91	0.11	8	2.94	0.12	5
FeI	5.35	0.10	8	5.37	0.10	5
FeII	5.29	0.06	8	5.40	0.10	5
CoI	2.94	0.18	6	3.00	0.15	5
NiI	4.12	0.13	8	4.12	0.09	5
CuI	1.49	0.14	8	1.53	0.13	5
ZnI	2.33	0.07	5	2.47	0.09	5
YII	−0.31	0.06	8	−0.23	0.06	5
BaII	−0.12	0.12	8	−0.09	0.15	5
CeII	−0.90	0.15	5	−0.84	0.12	5
NdII	−0.64	0.17	7[d]	−0.59	0.14	4
EuII	−1.44	0.15	6[d]	−1.32	0.34	5

[a] 8 RGB stars in NGC 2419 with [Mg/Fe] > 0 dex.
[b] 5 RGB stars in NGC 2419 with [Mg/Fe] < 0 dex. S1673 is taken as a RGB star; the changes in the means are very small if it is assumed to be on the AGB.
[c] The two strong Mg triplet lines are excluded.
[d] One upper limit is omitted.
[e] Based on Ca I lines in the HIRES spectra.
[f] Based on the 8542 and 8662 Å lines in Keck/DEIMOS spectra, see C10.
[g] The 4911 Å line of TiII is excluded.

galaxy stars are always accompanied by low abundances of other α elements, such as Si and Ca, where they signify the increasing role of (delayed) contributions from Type Ia supernovae, which are very effective at producing Fe-peak elements, to the chemical inventory. The situation in NGC 2419 is completely different, especially because Fe and other Fe-peak elements show no variation in NGC 2419.

3.1. *Consequences of the Large Range in Mg*

Ignoring H and He, the most abundant elements in a scaled solar mixture are C, N, O, Ne, Mg, Si, S, and Fe. Of these, C, N, O, Ne, and S all have high first ionization potentials, $\chi > 10$ eV. Thus, in the atmospheres of cool stars, Mg, Si, and Fe are the dominant sources of free electrons, and of these three, Mg has the lowest first ionization potential, and hence may be the most important. We have established that there is a substantial population of luminous giants in NGC 2419 with a very large deficiency of Mg. Given the potential importance of Mg to the structure of the stellar atmosphere, we must consider the potential implications of such a large deficiency. We investigated the structure of the model atmospheres, in part, in response to the suggestion by Mucciarelli et al. (2012) that the induced change in electron pressure, P_e, affects the CaT enough to produce the observed dispersion in line strengths in NGC 2419.

If the Mg abundance were to be increased from some initial level, one would expect P_e to rise, and to continue rising as the Mg abundance is increased further. However, decreasing the Mg abundance from some initial level does not produce the same behavior, as once Mg is sufficiently depleted, it will no longer be an effective electron donor compared to other sources of electrons, and any additional decrease in P_e will occur much more slowly. Thus, whatever the effect may be of the strong Mg depletion seen in the Mg-poor group of RGB stars in NGC 2419, we should not expect a very large range in behavior arising from the large range in the depletion of Mg within the Mg-poor population in NGC 2419.

One potential effect of a major change in the Mg abundance is that the position of the RGB in the CMD may shift depending on the Mg abundance to some extent. VandenBerg et al. (2012) recently evaluated the effects of altering the abundance of a single element drawn from a large list of suitable elements, including Mg. They found that increasing Mg by 0.4 dex at [M/H] $= -1.0$ substantially increases the opacity in the atmosphere and substantially shifts the RGB locus redder. However, at [M/H] $= -2$, the shift becomes much smaller, as can be seen by comparing their Fig. 7 to their Fig. 10 (the resulting opacity change) and their Fig. 15 to their Fig. 16

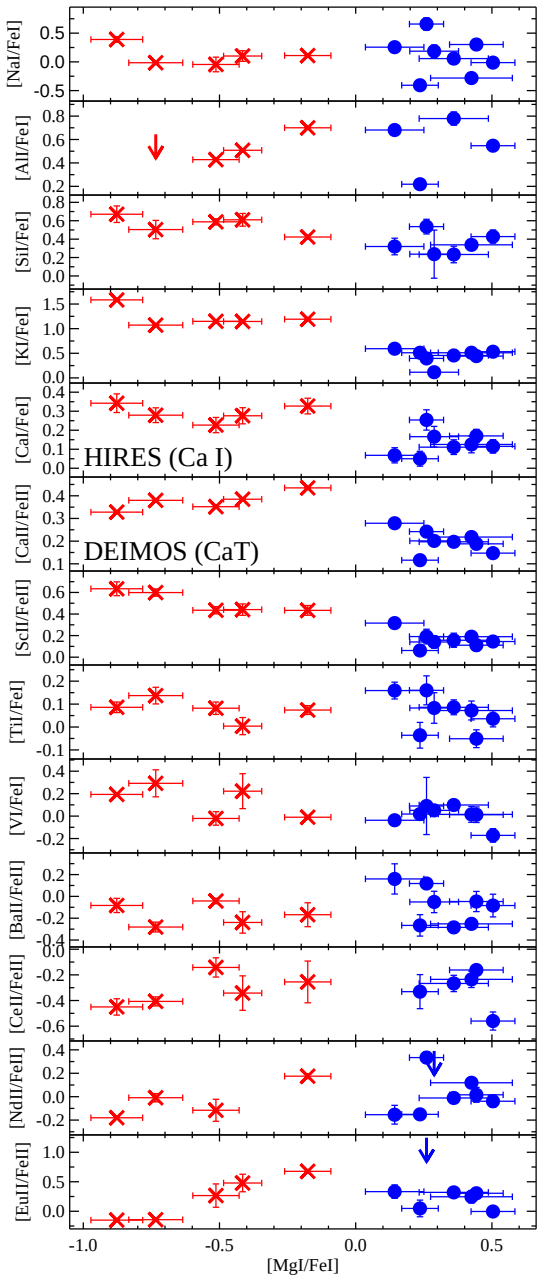

Figure 4. Abundance ratios for various species with respect to Fe, using Fe I or Fe II as appropriate, are shown as a function of [Mg/Fe] for our sample of 13 giants in NGC 2419 with HIRES spectra. Red crosses and blue points denote Mg-poor and Mg-rich giants respectively.

(the RGB positions in a CMD for these two values of [M/H] and for increases in Mg, Si, or Ca). In NGC 2419 where [M/H] ~ -2, the [Mg/Fe] value is deficient well below the normal α-enhanced value to one with [Mg/Fe] between -0.9 and -0.2 dex. It is clear from the calculations of VandenBerg et al. (2012) that the position of the RGB will *not* be perceptibly altered in this situation.

We initially expected, based on the substantial shifts in the RGB found by VandenBerg et al. (2012) at higher metallicity, that the Mg-rich and Mg-poor populations

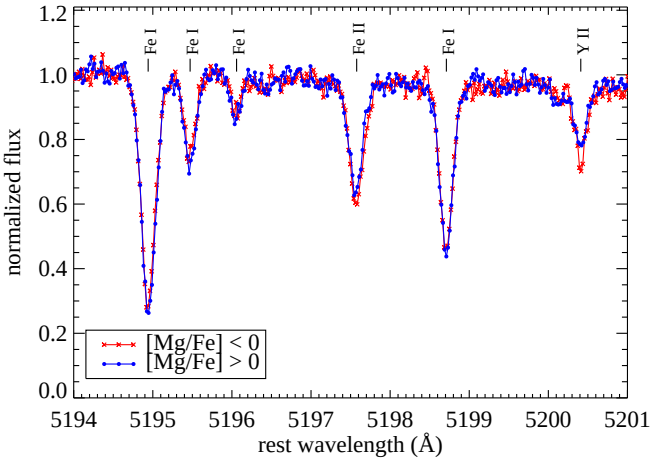

Figure 5. Sums of sections of spectra for the Mg-normal (blue points) and Mg-poor (red crosses) NGC 2419 giants centered on a group of Fe I lines and a Fe II line at 5197 Å. The two are indistinguishable. The sum for the Mg-normal stars omits S223, the most luminous and reddest NGC 2419 giant.

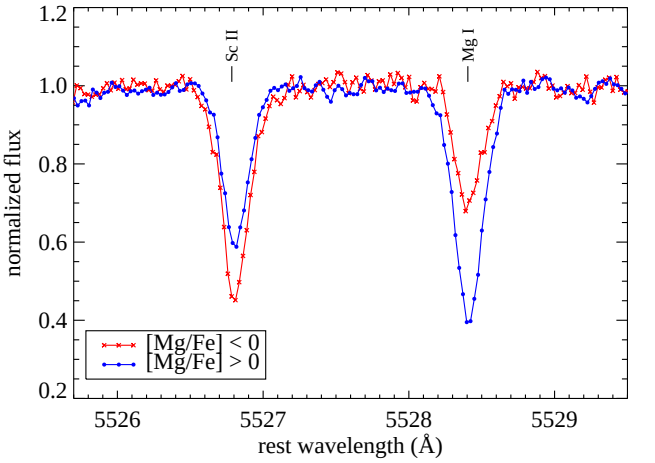

Figure 6. Sums of sections of spectra for the Mg-normal (blue points) and Mg-poor (red crosses) NGC 2419 giants centered on the Mg I line at 5528 Å and the Sc II line at 5526 Å. The extremely large difference in Mg abundance, as well as the somewhat smaller difference in Sc abundance, between the two groups is apparent. The sum for the Mg-normal stars omits S223, the most luminous and reddest NGC 2419 giant.

in NGC 2419 would be separated in the RGB with the Mg-poor population lying somewhat to the blue of the main RGB. However, CMDs using both $V-I$ and $V-J$ (see Fig. 1) show this is not the case. Understanding that no such shift is expected to happen for the specific case of NGC 2419 relieves our initial concern. It would maintain the validity of our normal methods of stellar parameter determinations, especially $T_{\rm eff}$, which rely on broad band colors. (However, we do not use colors here, instead relying on V alone.) It also gives specific guidance for the special case of the star S1673, which is the most Mg-depleted star in our sample. It lies somewhat to the blue in the V, $V-I$ CMD, but less so in V, $V-J$. Its location blueward of the RGB is either an unexpectedly large error in Stetson's (2005) visual photometry or is a reinforcement of our earlier suggestion that S1673 is an AGB star.

A second issue to consider is the effect of any decrease

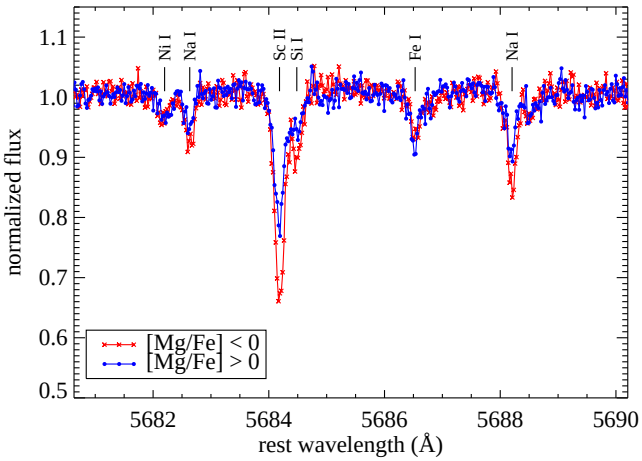

Figure 7. Sums of sections of spectra for the Mg-normal (red crosses) and Mg-poor (blue points) NGC 2419 giants centered on the Na I doublet at 5685 Å. Note that the Na I lines are only slightly stronger in the Mg-poor stars, while the adjacent Sc II and Si I lines are significantly stronger in those stars. The sum for the Mg-normal stars omits S223, the most luminous and reddest NGC 2419 giant.

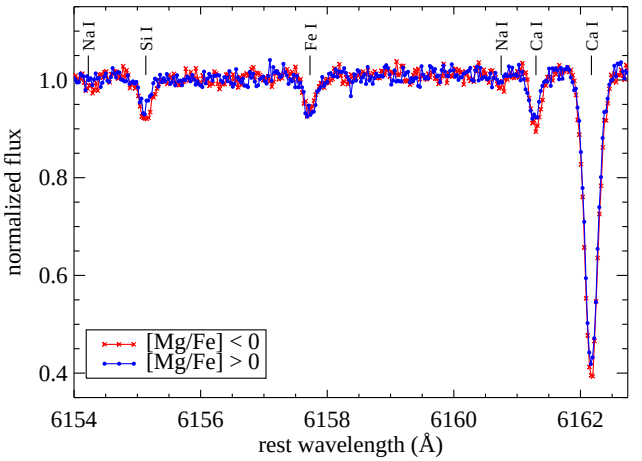

Figure 8. Sums of sections of spectra for the Mg-normal (red crosses) and Mg-poor (blue points) NGC 2419 giants centered on the Na I doublet at 6160 Å, which is so weak that it is barely detectable even in summed spectra. The adjacent Ca I and Fe I lines are almost identical between the Mg-poor stars and Mg-normal stars. The sum for the Mg-normal stars omits S223, the most luminous and reddest NGC 2419 giant.

in P_e on the formation of spectral lines. Because these are luminous cool giants, the temperatures are low, and most elements are mostly neutral. As a result, any decrease in P_e from a depletion of Mg will have little effect on the neutral lines, but the number density of the singly ionized species will rise. Is this the reason that the near-IR triplet, which is a line of Ca II, is enhanced in the Mg-poor population? The key question is whether P_e is affected by the decrease in Mg abundance within the stellar atmosphere, or whether the decrease in P_e at the metallicity of NGC 2419 is so small that there is no obvious change.

To this end, we calculated some model atmospheres at the stellar parameters characteristic of our NGC 2419 sample with Mg enhanced and depleted by 0.7 dex in each case. These tailored model atmospheres use as

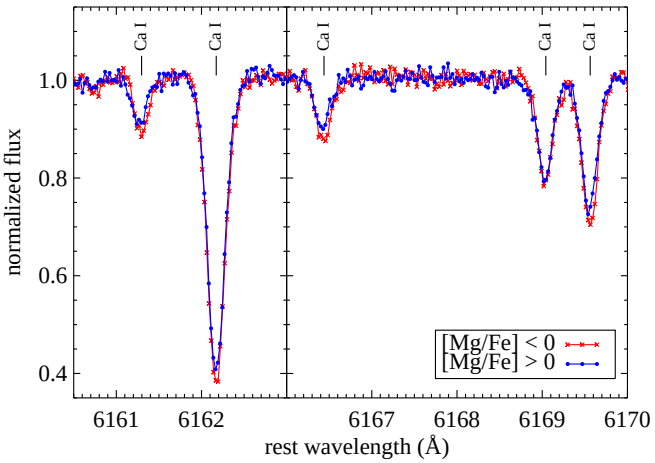

Figure 9. Sums of sections of spectra for the Mg-normal (red crosses) and Mg-poor (blue points) NGC 2419 giants covering several Ca I lines near 6165 Å. The Ca I lines are almost identical, with the lines of the Mg-poor group being slightly deeper. The sum for the Mg-normal stars omits S223, the most luminous and reddest NGC 2419 giant.

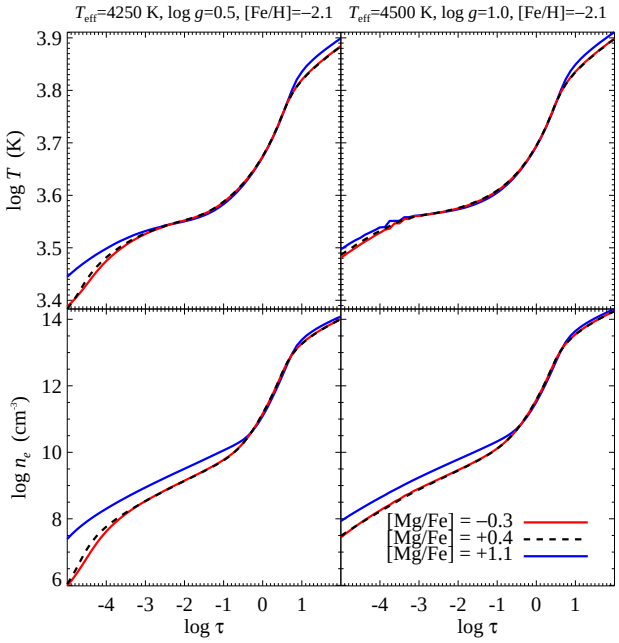

Figure 10. $T(\tau)$ and $n_e(\tau)$ are shown for stellar model atmospheres from Castelli & Kurucz (2004) that represent the Mg-normal population in NGC 2419 together with tailored models for Mg enhanced or depleted by a factor of 5. Note that n_e is identical for the Mg-normal and Mg-depleted models deeper than $\tau \sim 10^{-4}$, while the very highly Mg-enhanced models with [Mg/Fe] $\sim +1.1$ do show the expected trend of an increase in n_e at all optical depths deeper than $\tau \sim 10^{-4}$.

a base the α-enhanced models from Castelli & Kurucz (2004), which have scaled solar abundances but with $[\alpha/\mathrm{Fe}] = +0.4$, where all elements with even atomic number from O through Ti are considered α-elements. From this base composition the Mg abundance is perturbed up or down by a factor of 5 (0.7 dex) to construct new model stellar atmospheres.

Fig. 10 shows n_e and T as a function of τ for the base model atmospheres from Castelli & Kurucz (2004)

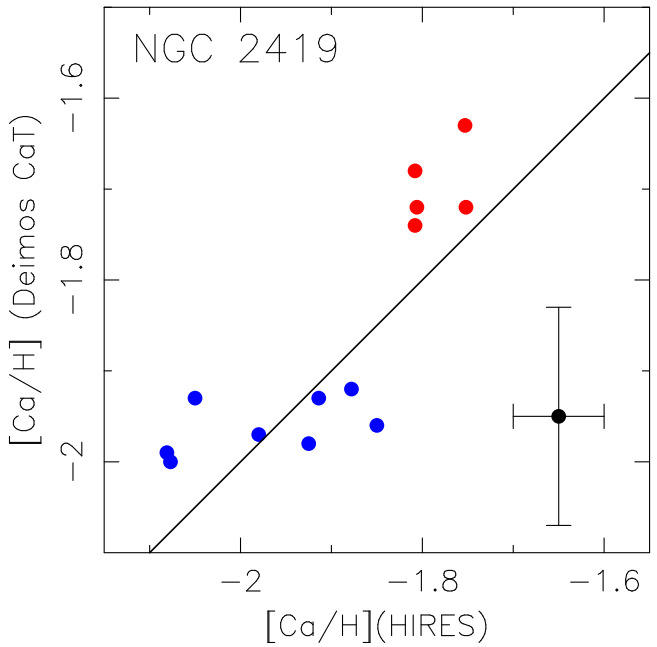

Figure 11. A comparison of the Ca abundance derived here from lines of Ca I for our sample of 13 RGB stars in NGC 2419 with Keck/HIRES spectra compared to that deduced by C10 from the infrared Ca triplet of Ca II. A line indicating equality is shown. A typical error bar is given in the lower right corner. Red and blue points denote Mg-poor and Mg-rich giants respectively.

(with [Mg/Fe] = +0.4), and for those with Mg further enhanced or depleted by a factor of 5 for two sets of stellar parameters, both with [M/H] = −2. The highly Mg-enhanced model (with [Mg/Fe] = +1.1) shows the expected behavior: a strong enhancement of n_e at all depths with $\tau > 10^{-4}$ compared to the base model. However, the Mg-depleted model closely follows the base model, implying that with such a large depletion of Mg, and given the low overall abundance of this GC of −2 dex, Mg is no longer an important source of free electrons. We might have expected this from the detailed isochrone calculations of VandenBerg et al. (2012), but it is gratifying that this is verified by our stellar model atmosphere calculations.

This agreement for $\tau > 10^{-4}$ suggests that our detailed abundance analyses which have been carried out using the base Castelli & Kurucz (2004) models will be valid for both the Mg-normal and the Mg-poor populations in NGC 2419, with the possible exception of lines formed higher in the atmosphere than $\tau = 10^{-4}$. None of the lines included in the detailed abundance analysis are strong enough for this to be the case. The only relevant spectral features that may be strong enough to be formed at so near the surface are the cores of the near-IR triplet of Ca II which were used in our DEIMOS analysis (C10) to suggest the possibility of a variation in the Ca abundance within NGC 2419. We note that any change in P_e does not affect the pressure broadening for lines strong enough to show damping wings as it is dominated by interactions with neutral H atoms (van der Waals broadening). It is the possible effect on the ionization balance for Ca via change in P_e that is of concern.

However, we reject the suggestion of Mucciarelli et al. (2012) that this is an important issue for NGC 2419 based on the good agreement between the abundance of neutral Ca lines presented here vs that from the near-IR triplet of Ca II presented by C10 (see Fig. 11), as well as from the evidence regarding the behavior of tailored model atmospheres as the Mg abundance is varied shown in Fig. 10. The prediction that there is no shift in the ionization equilibrium for the case of interest here means that achieving ionization equilibrium with the set of lines from the Keck/HIRES spectra used here is an important constraint that can be used to validate our detailed atmosphere abundance analyses. If NGC 2419 were more metal-rich by a factor of 4 or more, or Mg in the bulk of its population was more enhanced than we have established it to be, the consequences of differing Mg abundance between the two populations in this GC on P_e would become an important issue.

Although the Mg-poor stars in NGC 2419 also show a strong enhancement of potassium, K is less abundant than Mg in the solar mixture by a factor of ∼250, and so its enhancement by a factor of less than 10 in these stars will not produce any significant effect on the structure of the stellar atmosphere.

4. IS THERE A SPREAD IN ABUNDANCES WITHIN NGC 2419?

We have established that there are two groups of RGB stars in NGC 2419: those that appear like normal GC RGB stars with [Mg/Fe] ∼ +0.3 and a second group with extremely low Mg abundances (the Mg-poor group of 5 stars, with [Mg/Fe] ranging from −0.2 to −0.9 dex). Furthermore, the Mg-poor stars are those that have high Ca(CaT) from our Keck/DEIMOS study (C10). There is an anti-correlation with the K abundance such that the Mg-normal giants have [K/Fe] ∼ +0.4, a value consistent with that of other GCs and metal-poor halo stars (see, e.g., Cayrel et al. 2004 or Cohen et al. 2004, in which there are no non-LTE corrections), while the Mg-poor giants have [K/Fe] ∼ +1.1, a factor of 5 higher than the Mg-normal stars. The last element with detectable variations is Sc. As shown in Table 6 and in Fig. 5, there is no credible evidence for variation of Ti or any heavier Fe-peak element, including Fe itself.

4.1. *Mg and K*

Are the very large abundance variations seen among the NGC 2419 luminous RGB stars for Mg and K real? First, we discuss the case of Mg. There are three to five detected Mg I lines per star. The range in Mg abundance among the giants in our sample in NGC 2419 exceeds a factor of 10. There is no way that this can arise from a problem in the abundance analysis procedure. The non-LTE corrections for Mg I lines are small. Andrievsky et al. (2010) found that the typical correction for metal-poor giants is about +0.2 dex and not particularly sensitive to atmospheric parameters. Previous non-LTE computations reached similar results for disk stars (Mishenina et al. 2004) and for a range of stellar types and metallicities, down to [M/H] = −2 (Shimanskaya et al. 2000). All three of these studies used many of the same Mg I transitions that we used in our abundance analysis. We conclude that the variations in Mg abundance between the Mg-normal and Mg-poor stars must be real.

The situation with K is less clear. The variation of ϵ(K) in NGC 2419 (spanning a range of 1.4 dex) is large enough so that any inaccuracies caused by the stellar parameters or the analysis code are too small to produce the observed spread. However, the only lines of K that can be observed at optical wavelengths are the resonance doublet at 7665 and 7699 Å. Because the former is embedded deeply within a very strong terrestrial absorption band of O_2, it is practical to measure only the 7699 Å line. Given that this is a fairly strong resonance line, non-LTE corrections need to be considered.

Non-LTE corrections for the 7699 Å line of K I have been calculated by several groups (e.g., Ivanova & Shimanskiĭ 2000; Takeda et al. 2002; Andrievsky et al. 2010). The non-LTE corrections are negative, and range from −0.1 to −0.9 dex (see Fig. 6 of Ivanova & Shimanskiĭ 2000). They vary strongly with $T_{\rm eff}$ and with metallicity. Ivanova & Shimanskiĭ (2000) wrote that "the non-LTE corrections can vary strongly as functions of the model atmosphere parameters, which can sometimes be a source of substantial errors, even when comparing potassium abundances for stars of very similar type." It may be possible, with some contortions, to reproduce the behavior of K between the Mg-normal and Mg-poor stars in NGC 2419 with non-LTE corrections alone, but it does not seem likely.

Although the surveys of GC and halo field stars carried out prior to 2004, including the extensive work of the Lick-Texas group (e.g., Kraft 1994) and of Cohen and her collaborators (e.g., Cohen & Melendez 2005), did not include the K I lines due to limitations on spectral coverage, more recent work has found a small number of other metal-poor Galactic giants that show the very high K abundances of the Mg-poor giants in NGC 2419. Takeda et al. (2010) found two such stars in a survey of 15 RGB stars in three GCs. These two stars stick out in the same way as the K of the Mg-poor stars stick out in NGC 2419. One of these stars, M13 III–73, which has a [K/Fe] abundance 0.6 dex higher than the rest of the M13 sample, has been analyzed in detail by Kraft et al. (1992) and Pilachowski et al. (1996)[5]. They find that [Mg/Fe] = +0.25, a normal value for an α-enhanced GC star. Cayrel et al. (2004) found CS 30325–094, an EMP giant with [Fe/H] = −3.3, to have [K/Fe] = +0.72, with normal α-enhancement, and [Mg/Fe] and [Ca/Fe] both at +0.38 dex. (Note for future reference that [Sc/Fe] in this star is rather high at +0.33 dex.)

In summary, there are a few stars with [K/Fe] similar to those of the Mg-poor giants in NGC 2419, but they are not Mg-poor, in general. This suggests that the process generating K is not always tied to that producing the Mg-poor anomaly.

Takeda et al. (2010) suggested that some anomalously strong K resonance lines are caused by exceptional cases of strong peculiar velocity fields in the upper layers of the atmosphere and do not reflect the true K abundance of the star. To explore this possibility in our NGC 2419 sample, we measured the radial velocity of the K I 7699 Å line and compared it to that measured from other lines. We find that these agree for all 13 stars in our sample to within 0.5 km s^{-1} for all the stars except one, where the difference is 0.8 km s^{-1}. Furthermore, we used the Hα emission as a measure of chromospheric activity and possible mass loss. Cohen (1976) discovered that weak Hα emission is common in the brightest red giants in GCs. She interpreted the emission as mass loss from the bloated atmospheres of the giants. However, the implied mass loss rate was large. Dupree, Hartmann & Avrett (1984) later found from models of the atmospheres of red giants that static chromospheres can explain both the emission and the blueshift of Hα in bright, red giants. W_λ of the sum of the blue and red emission wings in Hα for luminous RGB stars in NGC 2419 are shown as a function of V (our proxy for $T_{\rm eff}$) in Fig. 12. Some of the sample stars show weak emission, but two stand out. The strongest Hα emission, which is extremely strong, is shown by S223, which is the most luminous and reddest RGB star in NGC 2419. It has obvious strong emission in both the red and blue wings of Hα and Hβ and also in the blue wings of Hγ and Hδ, as well as having broader metal lines than the other sample giants. The other case of strong emission is S1673, the star suspected to be on the AGB. Its emission is much weaker than S223 (see Fig. 12) but stronger than the other NGC 2419 giants in our sample. The Mg-poor stars behave no differently from the Mg-normal RGB stars in NGC 2419 in terms of their Hα emission. The mean radial velocity of Hα in the 5 Mg-poor stars differs from that of the metallic lines by only −0.3 km s^{-1}; the same value for the 8 Mg-normal stars in NGC 2419 is −0.6 km s^{-1}. The lithium line at 6707 Å cannot be detected in the summed spectra of either group of NGC 2419 giants. We therefore find untenable the suggestion that the high K seen in the Mg-poor giants in NGC 2419 arises from velocity fields in the outer layers of the stars. Furthermore, at the metallicity of NGC 2419, even for the Mg-poor, K-strong stars, the

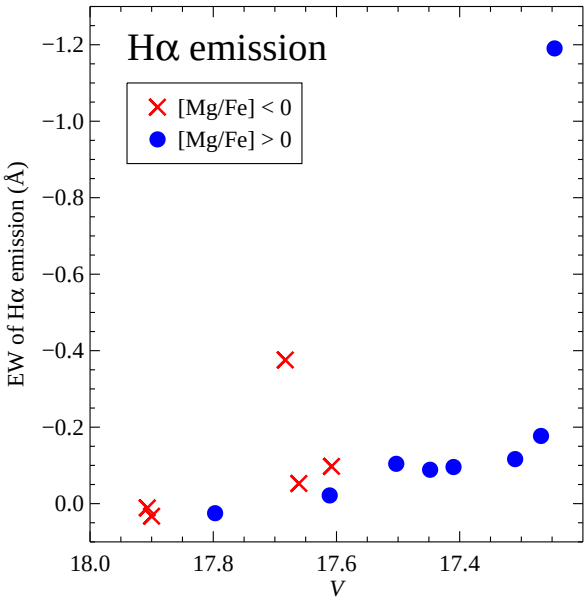

Figure 12. The sum of W_λ of emission in the blue and red wings of Hα as a function of V for our sample of luminous giants in NGC 2419. The red crosses indicate the Mg-poor stars, and the blue points represent the Mg-normal stars.

[5] We are trying to obtain a better HIRES spectrum of M13 III–73; it should be in hand shortly.

7699 Å line of K is not very strong, and most of it is not formed extremely high in the stellar atmosphere.

4.2. *Si, Ca, and Sc*

We now turn to elements which appear to show smaller variations within the stellar population of NGC 2419. According to Table 6 these are Si, Ca, and Sc. (The neutron capture elements may show a weakly significant dispersion, and we discuss them below.) Since there is the most information about Ca, we discuss it first.

The existence of Ca variations was first suggested by C10 based on their analysis of the strengths of the 8542 and 8662 Å lines (the two stronger lines of the CaT) from moderate resolution Keck/DEIMOS spectra of a large sample of stars. The key issue is whether this spread is caused by a real star-to-star abundance variation, or whether, since these features arise from singly ionized Ca, it is a consequence of a decrease in P_e due to the very low Mg abundances in the Mg-poor cluster giants. The present analysis (see Table 6) which is based on much higher resolution spectra from which typically 15 Ca I lines can be measured, also suggests a spread in Ca. Furthermore, C10 also presented the results of spectral syntheses using the method of Kirby et al. (2010) on the DEIMOS spectra, which specifically included Ca I lines in the appropriate wavelength region but excluded the CaT lines due to uncertainties in their line formation. Fig. 11 compares the Ca abundance derived here from Ca I features in our Keck/HIRES spectra with those derived by C10 from the infrared triplet lines of Ca II. The agreement is quite satisfactory; both show a small spread of ∼0.2 dex in Ca abundance with the Mg-poor population having a higher Ca abundance than the Mg-normal population in NGC 2419.

Variations in Ca abundance within a GC are quite unusual. Carretta et al. (2010) placed very tight limits on any variation in [Ca/H] of not more than 0.03 dex in a sample of 17 GCs. The only previously known GCs that show such variations are those suspected of being remnants of formerly accreted dwarf galaxies, such as ω Cen. From both spectroscopy and photometry, ω Cen has been known for more than 30 years to have a wide intrinsic range in [Ca/H], [Fe/H], and many other elements, extending over a range of ∼1.3 dex with multiple peaks in the metallicity distribution (Norris et al. 1996). Other GCs with spreads in [Fe/H] include M22 (Marino et al 2011) and NGC 1851 (Carretta et al. 2011).

One of the unresolved puzzles of C10 was the contrast between the constancy of [Fe/H] within the DEIMOS sample and the spread seen in Ca based on the strength of the near-IR triplet of Ca II. The present HIRES analysis confirms this surprising result, namely that there is no detectable spread in [Fe/H], yet there is a small one in [Ca/H] in NGC 2419. Those "globular clusters" such as ω Cen which do show variations in [Ca/H] within their stellar populations also show comparably large variations in [Fe/H]. The absence of a spread in Fe makes NGC 2419 unique in the details of its chemical inventory.

We considered the range of variation in Ca(CaT) as compared to the HIRES Ca I result. The means for [Ca/H] of the Mg-poor and the Mg-normal stars inferred from their HIRES spectra differ by 0.18 dex (see Table 6) while the difference for the same 13 stars for Ca(CaT) from our DEIMOS spectra (see Fig. 11) is somewhat larger, 0.27 dex. Nonetheless, the two independent values for the difference in Ca abundance between the Mg-poor and Mg-normal stars in NGC 2419 agree within the uncertainties. Furthermore, the Mg-poor and Mg-normal groups both show internal dispersions in Ca abundance that are considerably smaller than the difference between them. This applies to both the HIRES sample of 13 stars and the larger DEIMOS sample of C10.

Non-LTE corrections for Ca lines have been calculated by several groups, most recently by Spite et al. (2012). At the metallicity of NGC 2419 they are essentially zero and hence negligible for the subordinate Ca I lines, but that is not the case for the 4226 Å resonance line. Since the S/N at 4226 Å in our spectra is poor, we do not use the resonance line anyway. As a result, non-LTE effects are not an issue for the set of Ca I lines that we used for our present high-resolution study of luminous RGB stars in NGC 2419.

We therefore conclude that there is a real, but small, variation in Ca abundance between the Mg-poor and Mg-normal luminous giants in NGC 2419. The Mg-poor stars have a higher [Ca/H] abundance by ∼0.2 dex.

[Si/Fe] also shows a low amplitude anti-correlation with [Mg/Fe] such that the Mg-poor stars have values ∼0.2 dex higher than the Mg-normal stars in NGC 2419. This can be seen in Fig. 7.

The mean [Sc/Fe] we derive from our HIRES spectra of stars in NGC 2419 is 0.45 dex higher in the Mg-poor stars than in the Mg-poor stars. This difference is easily seen in the composite summed spectra of the Mg-poor and Mg-normal giants shown in Fig. 6 and in Fig 7 as well as in the plot of [Sc/Fe] vs. [Mg/H] shown in Fig. 4. We assert that the Sc abundance is noticeably different in the mean between the Mg-poor and Mg-normal groups of giants.

We note again that the Fe abundance is constant across both Mg-poor and Mg-normal giants in NGC 2419 to within 0.1 dex, as is shown in Table 6 and in Fig. 5. Carretta et al. (2009b) established strong upper limits on any star-to-star variation in [Fe/H] in a large sample of Galactic GCs. Only those GCs that are widely believed to be the remnants of accreted dwarf galaxies show star-to-star variations in [Fe/H].

4.3. *The Neutron Capture Elements*

Five of the heavy neutron capture elements (Y, Ba, Ce, Nd, and Eu) are detected in 10 or more of the 13 RGB stars in our HIRES sample for the GC NGC 2419, all as singly ionized species. The dispersion of [X/FeII] for these 6 elements is reasonably small considering that with the exception of Ba, for each of these species we have detected only a few weak lines redder than 4200 Å. Ba has four strong lines in the spectral region studied, most of which were detected in all the sample stars. Eu has a strong line at 4129 Å, but our spectra have low S/N there. So the abundance of Ba is the most reliable among these elements. The ratio of [Eu/Ba] for our sample of 13 RGB stars in NGC 2419 is +0.33 ±0.11 dex, comparable to that seen in other metal-poor GCs (see, e.g. Gratton, Sneden & Carretta 2004).

Table 6 demonstrates that there is no apparent difference exceeding 0.1 dex between abundances of any of these 6 elements between the Mg-poor and the Mg-

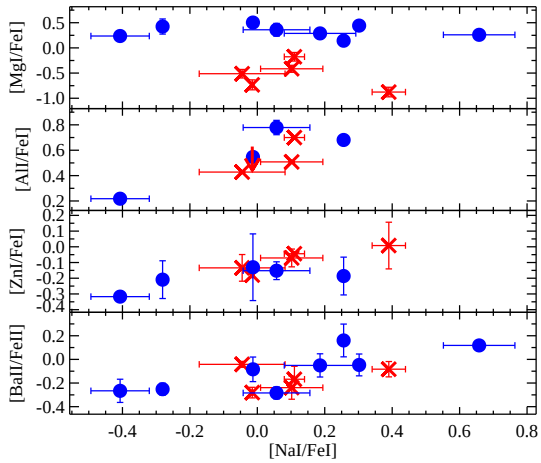

Figure 13. Abundance ratios for selected species with respect to Fe, using Fe I or Fe II as appropriate, are shown as a function of [Na/Fe] for our sample of 13 giants in NGC 2419 with HIRES spectra. The ratios selected are sensitive to proton burning chains operating among Na, Mg, and Al, and to a possible *s*-process contribution from intermediate-mass AGB stars. Red and blue points denote Mg-poor and Mg-rich giants respectively.

normal population in NGC 2419. However, as is shown in Fig. 13, there is a weak correlation between [NaI/FeI] and [BaII/FeII], and an even stronger correlation of [NaI/FeI] and [ZnI/FeI]. There is also a hint of a correlation between Al and Na, but the data are too sparse to be certain since the S/N at the strong Al I line at 3961 Å is too low to permit the use of that feature, and we must rely on the much weaker doublet at 6690 Å. No such correlation with any other element heavier than Fe with sufficient data was seen in our NGC 2419 sample. We may consider the Na abundance as a proxy for the typical mode of multiple populations involving proton-capture at high temperatures among the light elements seen in essentially all GCs as an anti-correlation between Na and O abundances. If we view the high Na abundance stars as those of the typical second generation, then we might consider the high Zn and Ba abundances as indicating a contribution from the *s*-process, such as was first seen in NGC 1851 by Yong & Grundahl (2008), who found that the Zr and La abundances of a small sample of stars were correlated with Al, and anti-correlated with O. Carretta et al. (2012b) present more recent results with a larger sample and find correlations between the Al and Ba abundances in this GC.

Thus NGC 2419 is unique among the GCs in that it has two distinct manifestations of multiple populations. The first is the classic proton burning at high T as manifested by correlations and anti-correlations among the light elements, seen in NGC 2419 as a range of Na abundances, and the related *s*-process contributions of Zn and Ba. The second is the strong Mg - K anti-correlation, which appears to have a completely separate origin.

5. POTENTIAL CAUSES OF THE ANOMALIES SEEN IN NGC 2419

In the previous section, we reviewed the evidence for anomalies in the chemical inventory of NGC 2419 and demonstrated that they are almost certainly real. They are not artifacts of analysis problems or non-LTE issues (except possibly for the enhancement of K, but probably not), and they require a nucleosynthetic explanation. We discuss these in order of the magnitude of the anomaly.

As reviewed by Gratton, Sneden & Carretta (2004), it is now well established that all GCs contain (at least) two generations of stars: the primordial generation, plus a second one whose light elements (C, N, O, Na, Mg, Al) show evidence for proton burning beginning with C and O burning into N, Ne burning into Na, and Mg burning into Al. Correlations and anti-correlations found among the light elements in GCs have demonstrated this high-temperature proton-burning occurs in the progenitors of the GC stars. A major study of these issues is summarized by Carretta et al. (2009a).

Furthermore, the light element abundance variations persist all the way down the RGB to the SGB and to and even below the main sequence turn-off (Briley et al. 1996). Thus, they cannot be attributed to stellar evolution within a single star, but must involve material processed in more massive stars, then ejected, with the usual suspects being intermediate mass AGB stars, as advocated by D'Antona et al. (2002) (see, e.g. D'Antona et al. 2012, for a more recent view), or rapidly rotating massive stars (Maeder & Meynet 2006). A low-amplitude correlation of Si with Al (∼0.2 dex increase in [Si/Fe] for [Al/Fe] increasing by 1.5 dex) is seen in a few GCs as well, e.g., Yong et al. (2005) and Carretta et al. (2012a), among others, implying proton burning occurring in even hotter environments.

AGB stars are also strong sites for the *s*-process, and thus the search for correlations with *s*-process element variations in GCs is also important. There are some hints that extensive proton burning producing very strong enhancements of Na (from Ne) and Al (from Mg) also produces small amounts of *s*-process material leading to correlations between small, marginally statistically significant enhancements of Y, Zr, and Ba with Na enhancements, as well as with much larger Al enhancements (Yong et al. 2005).

One might try to invoke a similar process to this to explain at least part of the anomalies in NGC 2419. However, Mg is a very abundant element, and in normal GCs, burning 40% of the original Mg will produce an enhancement of a factor of 10 or more in the Al abundance in the second generation stars. The burning of 90% of the Mg will produce an enhancement of Al which is much larger than that seen in the Mg-poor stars in NGC 2419. However, Fig. 13 demonstrates that while some of the usual correlations and anti-correlations among the light elements present in NGC 2419, the amplitude of the Al dispersion is by no means exceptional, as defined by the behavior of a sample of 15 GCs studied by Carretta et al. (2009a). It is especially puzzling that Mg itself does not correlate with Na, Al, Ba, or any other element typically indicative of proton burning or the *s*-process.

Furthermore, we have demonstrated that in the Mg-poor stars, K, Ca, and Sc, elements well beyond Si, are also enhanced. We rule out proton burning among the light elements as an explanation for the anomalies in the chemical inventory of NGC 2419 as it is impossible to reach the required temperature outside supernovae. Such burning may well be going on at a very low level, but it

is at best a minor contributor to the bizarre behavior we are trying to explain.

To explain the strong depletion of Mg seen in the Mg-poor population in NGC 2419 requires nuclear burning at high temperatures and beyond the range of nuclear processing believed to occur at the bottom of the surface convection zone in AGB stars. Mg is produced during the CNO cycle operating in the cores of massive stars, equivalent to $2\,^{12}\mathrm{C} \rightarrow\,^{24}$ Mg. It is also produced copiously in Type II supernovae. We have at present no explanation for the Mg-poor population.

Potassium is the one element discussed in this section where there is at least a semi-viable, non-nuclear explanation, namely non-LTE effects (see §4). But as discussed above, this is rather contrived, and probably cannot be made to work. Potassium is much less abundant in scaled solar mixtures than even Al, so if one tries to invoke proton burning cycles to produce the excess K seen in the Mg-poor population, a much larger enhancement of K is predicted than is observed.

K is primarily produced by oxygen burning in Type II SNe, but, as discussed by Clayton (2003), its production depends heavily on the progenitor mass and on the assumptions regarding fallback and when material is ejected during the SN explosion. Scandium is even rarer than K in a scaled solar mixture, and its abundance in Type II SN ejecta depends crucially on how far oxygen burning has proceeded in material before it is ejected. Varying only the progenitor mass, the Type II SN yields of Nomoto et al. (2006) show a peak in production of both K and Sc with respect to Ca for a Type II SN progenitor mass of between 18 and 20 $M_{\odot}$ depending on the initial metallicity (zero or low) of the SN progenitor. Given this, it may be possible, by tinkering with the characteristics of Type II SN explosions, to produce highly varying fractions of K and of Sc in the ejecta. Since the yields of K and Sc given by Nomoto et al. (2006) vary more or less together, one might expect to see correlated abundances of K and Sc, as is the case in NGC 2419.

The dominant isotope of Si is ^{28}Si, which can be assembled from 7 nuclei of ^{4}He. It is very tightly bound and is the primary product of O burning in the cores of massive stars. The dominant isotope of Ca is ^{40}Ca, which has the magic number 20 of both protons and neutrons. Thus, it is very stable compared to its neighbors in the periodic table of the elements. It can be assembled from 10 nuclei of ^{4}He. It, too, is produced primarily in Type II SNe during O burning. The abundances of these very stable elements in Type II SN ejecta are less sensitive to the details of the explosion than those of K or Sc. This may be why the mean differences in abundance between the Mg-poor and Mg-normal populations in NGC 2419 for Si and Ca are just 0.2 dex between the two groups.

Type II SN nucleosynthesis models including ejection mechanisms, fallback, and mixing within the ejecta can successfully explain the chemical inventory of (most) EMP Galactic halo stars (Kobayashi et al 2006; Tominaga, Umeda & Nomoto 2007; Heger & Woosley 2010). If one wishes to invoke peculiar Type II SN explosions to explain the anomalies in the chemical inventory of NGC 2419, since it is (even now) a very massive GC, just one peculiar Type II SN may not eject enough material to produce a population of Mg-poor stars which comprises ∼30% of the present cluster stars. Speculation that multiple, peculiar Type II SNe occurred in NGC 2419 and in no other known GC seems rather ad hoc and therefore unsatisfactory.

6. BROADER IMPLICATIONS OF THE LARGE MG VARIATIONS IN NGC 2419

The depletion of Mg among the Mg-poor stars we have found in NGC 2419 is unprecedented among metal-poor stellar systems of any age or total mass. VandenBerg et al. (2012) calculated the effect of single-element enhancements on GC isochrones. At the low metallicity ([Fe/H] ~ -2.1) of this GC, they found very small changes on the RGB position in the CMD. At higher metallicity, VandenBerg et al. (2012) found substantial changes in the positions of the RGB in a simple stellar population such as GC. Furthermore, augmentations in Mg (or Ca) relative to Fe would have even larger consequences than depletions. The same holds true for the effects induced by a change in the abundance of a specific element with regard to the line strengths of individual spectral features, both those of the element involved, and those of other elements through the effect of a change in P_e and hence a change in ionization ratios. Spectral features originating from an ionization stage which contains only a small fraction of the total atoms of the relevant element can be significantly altered in strength. The RGB plus AGB dominate the total light at optical and IR wavelengths in old stellar populations. In these cool stars, it is the population and potentially the line strength of the neutral vs. the singly ionized species that may be affected.

If large divergences in the abundance of a single (abundant, low first ionization potential) element from the scaled solar ratio or the normal α-enhanced ratio do occur in simple stellar systems, then the consequences for the study of more distant stellar systems, where only the integrated light can be observed, may be profound. For example, the calibrations relating [M/H] and the Mg triplet line indices for the Lick indices (Worthey & Ottaviani 1997; Puzia, Perrett & Bridges 2005), widely used to interpret moderate resolution spectra of galaxies and GCs beyond the Local Group, will be altered. Substantial star-to-star variation within a GC of the abundances of crucial elements could mimic a variation of overall metallicity or an age spread. By increasing the number of parameters that must be considered, possible variations in the abundances of key individual elements add considerable complexity to the interpretation of the their CMDs.

So far only NGC 2419 shows such behavior in its chemical inventory, and since this is such a metal-poor GC, the effects on its CMD are very small, and the effects on its spectrum only appear in the lines of elements that are actually abnormal in their abundances. While finding many more such cases, especially at higher metallicity, would be very interesting, for the sake of our entire knowledge base of the composite light of simple stellar systems, we must hope that such cases are very rare.

7. SUMMARY

Our initial work on the extremely distant and massive outer halo GC NGC 2419 (C10) used moderate resolution spectra from Keck/DEIMOS. We suggested the presence of a star-to-star spread in [Ca/H] but no detectable

spread in [Fe/H] based on an analysis of the strong Ca II near-IR triplet and spectral synthesis of weaker, neutral lines. We then proceeded (C11) to obtain high-dispersion spectra of a sample of stars, most of which appeared to be normal, α-enhanced red giants similar to those found in most GCs. But C11's sample also contained one very peculiar star, S1131, which showed very depleted Mg and highly enhanced K and was apparently Ca-rich as well. To follow this up, in this paper we presented abundance analyses of 6 new RGB stars in NGC 2419, most selected to be among the most apparently Ca enhanced in the study of C10.

We found that there are two groups of stars in NGC 2419, one of which is identical to the typical GC α-enhanced RGB stars. The second group, which contains roughly 1/3 of the stellar population of this GC, is very peculiar. These stars have extremely depleted Mg, ranging down to -0.9 dex below the Solar ratio, i.e., about a factor of 15 below the normal-Mg stars. These Mg-poor stars are identical to those with apparently high Ca from C10, and from the present detailed abundance analyses show highly enhanced K, moderately enhanced Sc, and a small enhancement of Si and Ca compared to the Mg-normal stars. But there is no credible evidence for any variation of [Fe/H] within this GC. This chemical inventory is unprecedented and unique.

We discussed whether some of this behavior, in particular the apparent enhancement in Ca, can be attributed to low P_e in the stellar atmosphere arising from the depletion of Mg, an important electron donor at low temperature when H is neutral. We concluded that the small difference in Ca abundance (~ 0.2 dex) between the Mg-poor and Mg-normal giants is real.

A number of suggestions have been offered for for producing some of these peculiarities, which do very rarely occur in other GC and field halo stars, without invoking a real difference in chemical inventory between the Mg-poor and Mg-normal giants. We provided evidence against the suggestion by Takeda et al. (2010) that unusually strong turbulence in the upper atmospheres of the stars might produce the apparent excess of K, at least in the case of NGC 2419. We looked at the variation with stellar parameters and with metallicity of the non-LTE corrections for each of the relevant elements. In the end, we concluded that all of these variations, correlations, and anti-correlations involving Mg, K, Sc, Ca, and Si are real differences in mean abundances between the Mg-poor and Mg-normal population.

It is not too difficult to imagine slightly altering the characteristics of Type II SNe (their mass distribution, the explosion energy, the fallback, etc.) to reproduce the behavior of Sc and K. We have not found a similar solution for Mg, Ca, and Si. Even the explanation for Sc and K is unsatisfactory because it requires multiple Type II SNe to be peculiar with respect to those SNe that produced the material in all other known GCs.

In addition to the Mg-K anti-correlation and related issues that we have found, there is evidence that the usual correlations and anti-correlations among the light elements characteristic of proton-burning at high temperature that are seen in most GCs are present in NGC 2419 as well, and may be accompanied by s-process enhancements among some of the heavy neutron capture elements. But the two signs of multiple populations act independently in NGC 2419; the Na-poor and Na-rich giants do not correspond at all with the Mg-poor and Mg-normal giants in this peculiar GC.

With the present work, we now have a clear view of the complex chemical inventory within NGC 2419 and of the extremely peculiar Mg-poor population which which contains roughly 1/3 of its stellar population. However, we have not found a solution to the puzzle of how to reproduce through nuclear reactions the characteristics of the Mg-poor population in NGC 2419. One puzzle was unveiled by C10, C11, and the present work, but another has now been revealed and is at present without any satisfactory solution.

With this new evidence demonstrating the uniqueness of NGC 2419 among the Milky Way system of GCs, we repeat the suggestion we made in C10 that NGC 2419 is not a GC. Instead, it may be the nucleus of a disrupted dwarf galaxy. Although it presently has no dark matter (Baumgardt et al. 2009) and a gravitational potential well unlikely to retain supernova ejecta, it may have previously resided in a dark matter halo, such as an accreted dwarf galaxy. M54, the core of the Sagittarius dwarf spheroidal galaxy, likely shares the same origin (Sarajedini & Layden 1995), and a similar story has been suggested for ω Cen (Lee et al. 1999). If NGC 2419 joins this growing category of clusters, then it will be unique among its class for retaining some (e.g., Ca, Sc, K) but not all (e.g., Fe) supernova products.

We are grateful to the many people who have worked to make the Keck Telescope and its instruments a reality and to operate and maintain the Keck Observatory. The authors wish to extend special thanks to those of Hawaiian ancestry on whose sacred mountain we are privileged to be guests. Without their generous hospitality, none of the observations presented herein would have been possible. We thank Stan Woosley for a helpful conversation on the nucleosynthetic origin of potassium. J.G.C. thanks NSF grant AST-0908139 for partial support. Work by E.N.K. was supported by NASA through Hubble Fellowship grant HST-HF-01233.01 awarded to E.N.K. by the Space Telescope Science Institute, which is operated by the Association of Universities for Research in Astronomy, Inc., for NASA, under contract NAS 5-26555.

REFERENCES

Andrievsky, S. M., Spite, M., Korotin, S. A., Spite, F., Bonifacio, P., Cayrel, R., Francois, P. & Hill, V., 2010, A&A, 13223
Baumgardt, H., Côté, P., Hilker, M., et al. 2009, MNRAS, 396, 2051
Baumüller, D. G. & Gehren, T., 1997, A&A, 325, 1088
Briley, M. M., Smith, V. V., Suntzeff, N. B., et al. 1996, Nature, 383, 604
Carretta, E., Bragaglia, A., Gratton, R.& Lucatello, S., 2009, A&A, 505, 117
Carretta, E., Bragaglia, A., Gratton, R., D'Orazi, V. & Lucatello, S., 2009, A&A, 508, 695
Carretta, E., Lucatello, S., Gratton, R. G., Bragaglia, A. & D'Orazi, V., 2011, A&A, 533, A69
Carretta, E., Bragaglia, A., Gratton, R., Lucatello, S., Bellazzini, M. & D'Orazi, V., 2010, ApJ, 712, L21
Carretta, E., Bragaglia, A., Gratton, R., Lucatello, S. & D'Orazi, V., 2012, ApJ, in press (arXiv:1204.0259)
Carretta, E., D'Orazi, V., Gratton, R. G. & Lucatello, S., 2012, A&A, in press
Castelli, F. & Kurucz, R. L., 2004, astro-ph/0405087
Cayrel, R. et al, 2004, A&A, 416, 1117
Clayton, D., 2003, *Handbook of Isotopes in the Cosmos*, Cambridge University Press, Cambridge, United Kingdom

Cohen, J. G., 1976 ApJ, 203, L127
Cohen, J. G., Christlieb, N., McWilliam, A., Shectman, S., Thompson, I., Wasserburg, G., Ivans, I., Dehn, Karlsson, T. & Melendez, J., 2004, ApJ, 612, 1107
Cohen, J. G. & Melendez, J., 2005, AJ, 129, 303
Cohen, J. G. & Huang, W., 2010, ApJ, 719, 931
Cohen, J. G., Kirby, E. N., Simon, J. & Geha, M., 2010, ApJ, 725, 288 (C10)
Cohen, J. G., Huang, W. & Kirby, E. N., 2011, ApJ, 740, 60 (C11)
Cutri, R. M. et al, 2003, "Explanatory Supplement to the 2MASS All-Sky Data Release, http://www.ipac.caltech.edu/2mass/releases/allsky/doc/explsup.html
D'Antona, F., Caloi, V., Montalbán, J., Ventura, P., & Gratton, R. 2002, A&A, 395, 69
D'Antona, F., D'Ercole, A., Carini, R., Vesperini, E. & Venture, P., A&A, in press (arXiv:1207.1544)
di Criscienzo, M., D'Antona, F., Milone, A. P., et al. 2011, MNRAS, 414, 3381
Dupree, A.K, Hartmann, L. & Avrett, E.H., 1984, ApJ, 281, L37
Gratton, R., Sneden, C. & Carretta, E., 2004, ARA&A, 42, 385
Harris, W. E., Bell, R. A., VandenBerg, D. A., et al. 1997, AJ, 114, 1030
Heger, A. & Woosley, S. E., 2010, ApJ, 724, 341
Ibata, R. A., Gilmore, G., & Irwin, M. J. 1995, MNRAS, 277, 781
Ibata, R., Sollima, A., Nipoti, C., et al. 2011, ApJ, 738, 186
Ivanova, D. V. & Shimanskiĭ, V. V., 2000, Astronomy Reports, 44, 376
Kirby, E. N., Cohen, J. G., Smith, G. H., et al. 2011, ApJ, 727, 79
Kirby, E. N., Guhathakurta, P., Simon, J. D., et al. 2010, ApJS, 191, 352
Kobayashi, C., Umeda, K., Nomoto K., Tominaga, N. & Ohkubo, T., 2006, ApJ, 653, 1145
Kraft, R. P. 1994, PASP, 106, 553
Kraft, R. P., Sneden, C., Langer, G. E. & Prosser, C. F.. 1992, AJ, 104, 645
Kurucz, R. L., 1993, ATLAS9 Stellar Atmosphere Programs and 2 km/s Grid, (Kurucz CD-ROM No. 13)
Lee, Y.-W., Joo, J.-M., Sohn, Y.-J., et al. 1999, Nature, 402, 55
Letarte, B., Hill, V., Tolstoy, E., et al. 2010, A&A, 523, A17
Marino, A. F. et al, 2011, A&A, 532, A8
Maeder, A. & Meynet, G., 2006, A&A, 448, L37
Mishenina, T. V., Soubiran, C., Kovtyukh, V. V., & Korotin, S. A. 2004, A&A, 418, 551
Mucciarelli, A., Bellazzini, M., Ibata, R., Merle, T. & Chapman, S. C., 2012, MNRAS, submitted
Nomoto, K., Tominaga, N., Umeda, H., Kobayashi, C., & Maeda, K. 2006, Nuclear Physics A, 777, 424
Norris, J. E., Freeman, K. C. & Mighell, K. J., 1996, ApJ, 462, 241
Pilachowski, C. A., Sneden, C., Kraft, R. P. & Langer, G. E., 1996, AJ, 112, 545
Puzia, T. H., Perrett, K. M. & Bridges, T. J., 2005, A&A, 434, 090
Sarajedini, A., & Layden, A. C. 1995, AJ, 109, 1086
Shetrone, M., Côté, P. & Sargent, W. L. W., 2001, ApJ, 568, 592
Shimanskaya, N. N., Mashonkina, L. I., & Sakhibullin, N. A. 2000, Astronomy Reports, 44, 530
Skrutskie, M. F. et al, 2006, AJ, 131, 1163
Sneden, C., 1973, Ph.D. thesis, Univ. of Texas
Sobeck, J. S. et al, 2011, AJ, 141, 175
Spite, M., Andrievsky, S M., Spite, F. et al, 2012, A&A, in press (arXiv:1204.1139)
Stetson, P. B., 2005, PASP, 117, 563
Suntzeff, N. B., Kraft, R. P., & Kinman, T. D. 1988, AJ, 95, 91
Takeda, Y., Zhao, G., Chen, Y. Q., Qui, H. M. & Takada-Hidai, M., 2002, PASJ,54,275
Takeda, Y., Kaneko, H., Matsumoto, N., Oshino, S., Ito, H. & Shibuya, T., 2010, PASJ, 61, 563
Tominaga, N., Umeda, H. & Nomoto, K., 2007, ApJ, 660, 516
VandenBerg, D. A., Bergbusch, P. A., Dotter, A., Ferguson, J., Michaud, G., Richer, J. & Profitt, C. R., 2012,, ApJ, in press (arXiv:126.1820)
Vogt, S. E. et al. 1994, SPIE, 2198, 362
Worthey, G. & Ottaviani, D. L., 1997, ApJS, 111, 377
Yi, S., Kim, Y.-C., Demarque, P. & Alexander, D. R., 2003, ApJS, 143, 499
Yong, D., Grundahl, F., Nissen, P. E., Jensen, H. R. & Lambert, D. L., 2005, 2005, A&A, 438, 875
Yong, D. & Grundahl, F., 2008, ApJ, 672, L29

Table 4
Abundances for First 6 Red Giant Members of NGC 2419 With Keck/HIRES Spectra

Elem	Sun (dex)	S1131 [X/Fe][b] (dex)	S1131 σ[c] (dex)	S1131 N	S1004 [X/Fe] (dex)	S1004 σ (dex)	S1004 N	S1065 [X/Fe] (dex)	S1065 σ (dex)	S1065 N	S458 [X/Fe] (dex)	S458 σ (dex)	S458 N	S1673 [X/Fe] (dex)	S1673 σ (dex)	S1673 N	S1673[a] [X/Fe] (dex)	S1673[a] σ (dex)	S1673[a] N	S1814 [X/Fe] (dex)	S1814 σ (dex)	S1814 N
C(CH)[d]	8.59	−0.73	···	1	−0.55	···	1	−0.78	···	1	−0.95	···	1	−1.00	···	1	−1.04	···	1	−0.77	···	1
Na I	6.32	−0.05	0.18	2	0.08	0.02	2	−0.02	···	1	0.10	0.16	3	0.44	0.08	2	0.39	0.07	2	−0.01	···	1
Na I[e]	6.32	···	···	···	···	···	···	···	···	···	0.04	0.12	2	···	···	···	···	···	···	···	···	···
Mg I	7.54	−0.51	0.19	5	−0.16	0.29	2	−0.73	0.14	2	−0.42	0.14	4	−0.86	0.17	4	−0.88	0.19	4	0.60	0.18	3
Mg I[f]	7.54	−0.54	0.24	3	···	···	···	···	···	···	−0.41	0.06	2	−1.03	0.09	2	−1.08	0.10	2	···	···	···
Al I	6.47	0.43	···	1	0.70	···	1	≤0.44	···	1	0.51	···	1	···	···	···	···	···	···	0.55	···	1
Si I	7.55	0.59	0.12	13	0.42	0.03	2	0.50	0.20	4	0.61	0.12	3	0.79	0.17	3	0.67	0.18	4	0.43	0.16	5
K I	5.12	1.15	···	1	1.19	···	1	1.07	···	1	1.15	···	1	1.55	···	1	1.58	···	1	0.53	···	1
Ca I	6.36	0.23	0.17	18	0.33	0.16	15	0.28	0.15	15	0.28	0.17	16	0.37	0.22	15	0.34	0.19	15	0.11	0.15	18
Sc II	3.10	0.40	0.09	7	0.45	0.12	7	0.53	0.09	7	0.40	0.14	7	0.89	0.23	7	0.67	0.17	7	0.19	0.13	8
Ti I	4.99	0.08	0.13	23	0.07	0.07	13	0.14	0.15	17	0.00	0.14	14	0.00	0.10	12	0.09	0.08	12	0.04	0.17	23
Ti II	4.99	0.38	0.26	9	0.09	0.30	6	0.30	0.07	5	0.15	0.25	6	−0.01	0.29	5	0.04	0.29	5	0.43	0.16	6
V I	4.00	−0.02	0.12	4	−0.01	···	1	0.29	0.17	2	0.22	0.22	2	0.08	···	1	0.19	···	1	−0.17	0.12	4
Cr I	5.67	−0.24	0.15	6	−0.26	0.07	5	−0.26	0.20	4	−0.35	0.11	5	−0.36	0.09	5	−0.30	0.10	5	−0.35	0.17	6
Mn I	5.39	−0.34	0.12	7	−0.38	0.09	5	−0.32	0.08	5	−0.33	0.09	5	−0.47	0.20	5	−0.43	0.09	5	−0.35	0.07	6
Fe I[g]	7.45	−2.03	0.15	107	−2.08	0.14	75	−2.03	0.15	82	−2.08	0.15	74	−2.18	0.11	57	−2.04	0.13	57	−2.19	0.14	92
Fe II[h]	7.45	−0.04	0.20	11	0.02	0.23	10	−0.07	0.16	11	−0.04	0.26	12	0.30	0.27	4	0.04	0.23	4	0.05	0.21	14
Co I	4.92	0.11	0.12	3	0.32	0.22	2	0.25	0.06	2	0.01	···	1	0.13	···	1	0.17	···	1	···	···	···
Ni I	6.25	−0.04	0.18	18	−0.04	0.22	15	0.00	0.21	16	−0.08	0.25	16	−0.08	0.18	15	−0.07	0.18	15	−0.08	0.20	21
Cu I	4.21	−0.70	···	1	−0.50	0.20	2	−0.51	···	1	−0.61	···	1	−0.68	···	1	−0.64	···	1	−0.60	···	1
Zn I	4.60	−0.13	0.12	2	−0.04	0.01	2	−0.18	0.02	2	−0.07	0.08	2	0.20	0.22	2	0.01	0.21	2	−0.13	0.30	2
Sr I	2.90	···	···	···	···	···	···	−0.56	···	1	···	···	···	···	···	···	···	···	···	−0.20	···	1
Sr II	2.90	−0.37	···	1	···	···	···	···	···	···	···	···	···	···	···	···	···	···	···	−0.15	···	1
Y II	2.24	−0.41	0.10	3	−0.38	0.11	3	−0.53	0.08	5	−0.39	0.19	5	−0.20	0.06	3	−0.38	0.11	3	−0.37	0.12	4
Ba II	2.13	−0.04	0.05	4	−0.17	0.19	3	−0.28	0.09	4	−0.24	0.17	3	−0.14	0.17	3	−0.08	0.13	4	−0.08	0.18	3
La II	1.14	0.04	···	1	···	···	···	···	···	···	···	···	···	···	···	···	···	···	···	−0.04	···	1
Ce II	1.55	−0.14	0.13	3	−0.26	0.23	2	−0.41	0.05	2	−0.34	0.19	2	−0.57	0.09	2	−0.45	0.09	2	−0.56	0.10	2
Nd II	1.50	−0.12	0.21	5	0.17	0.03	2	−0.01	0.05	2	···	···	···	−0.30	0.06	2	−0.18	0.02	2	−0.04	0.09	3
Eu II	0.51	0.27	0.28	2	0.68	···	1	−0.14	···	1	0.48	0.21	2	−0.20	···	1	−0.15	···	1	0.00	0.11	2
Dy II	1.10	···	···	···	···	···	···	···	···	···	···	···	···	···	···	···	···	···	···	0.34	···	1

[a] This is the AGB solution for S1673.
[b] [X/Fe]: Fe I is used for neutral species, Fe II for ionized species.
[c] The rms dispersion about the mean of [X/Fe].
[d] From synthesis of the CH band near 4320 Å.
[e] The strong Na D lines are omitted.
[f] The strong Mg triplet lines are omitted.
[g] This is [Fe(Fe I)/H].
[h] This is [Fe(Fe II)/Fe(Fe I)]].

Table 5
Abundances for Last 7 Red Giant Members of NGC 2419 With Keck/HIRES Spectra

Elem	Sun (dex)	S1166 [X/Fe][a] (dex)	S1166 σ[b] (dex)	S1166 N	S406 [X/Fe][a] (dex)	S406 σ[b] (dex)	S406 N	S1209 [X/Fe][a] (dex)	S1209 σ[b] (dex)	S1209 N	S223 [X/Fe][a] (dex)	S223 σ[b] (dex)	S223 N	S810 [X/Fe][a] (dex)	S810 σ[b] (dex)	S810 N	S1305 [X/Fe][a] (dex)	S1305 σ[b] (dex)	S1305 N	S973 [X/Fe][a] (dex)	S973 σ[b] (dex)	S973 N
C(CH)[c]	8.59	−0.73	···	1	−0.76	···	1	−0.74	···	1	−0.93	···	1	−0.86	···	1	−0.31	0.20	0	···	···	···
[O I]	8.83	···	···	···	···	···	···	0.70	···	1	···	···	···	0.24	0.25	2	···	···	···	0.75	0.04	2
Na I	6.32	−0.28	···	1	0.06	0.14	2	0.30	···	1	0.26	0.02	2	−0.41	0.15	3	0.66	0.15	2	0.19	0.15	2
Na I[d]	6.32	···	···	···	···	···	···	···	···	···	···	···	···	−0.50	0.11	2	···	···	···	···	···	···
Mg I	7.54	0.42	0.26	3	0.36	0.22	3	0.44	0.22	5	0.14	0.24	5	0.24	0.15	5	0.26	0.14	5	0.29	0.20	5
Mg I[e]	7.54	···	···	···	···	···	···	0.50	0.13	3	0.09	0.34	3	0.23	0.18	3	0.24	0.15	3	0.33	0.27	3
Al I	6.47	···	···	···	0.78	0.08	2	···	···	···	0.68	···	1	0.22	···	1	···	···	···	···	···	···
Si I	7.55	0.34	0.08	3	0.23	0.18	4	···	···	···	0.32	0.18	4	···	···	···	0.54	0.16	4	0.24	0.37	2
K I	5.12	0.51	···	1	0.46	···	1	0.44	···	1	0.59	···	1	0.51	···	1	0.40	···	1	0.12	···	1
Ca I	6.36	0.12	0.17	15	0.11	0.14	13	0.17	0.13	14	0.07	0.15	14	0.05	0.13	11	0.25	0.20	14	0.17	0.21	15
Sc II	3.10	0.05	0.11	7	0.05	0.16	6	0.18	0.13	6	0.18	0.09	7	0.01	0.09	7	0.15	0.18	7	0.00	0.15	7
Ti I	4.99	0.07	0.16	15	0.09	0.13	16	−0.05	0.16	17	0.16	0.16	19	−0.04	0.21	14	0.16	0.20	10	0.08	0.20	9
Ti II	4.99	0.20	0.07	5	0.02	0.21	5	0.30	0.15	10	0.28	0.29	5	0.00	0.26	7	0.17	0.29	5	0.05	0.26	4
V I	4.00	0.01	0.14	4	0.10	···	1	0.01	0.12	3	−0.04	0.13	9	0.02	0.08	3	0.09	0.36	2	0.05	0.07	3
Cr I	5.67	−0.35	0.22	4	−0.34	0.18	4	−0.38	0.12	6	−0.29	0.21	5	−0.39	0.15	4	−0.49	0.20	2	−0.27	0.04	2
Mn I	5.39	−0.41	0.09	5	−0.39	0.09	5	−0.37	0.14	6	−0.43	0.12	6	−0.44	0.12	6	−0.40	0.10	6	−0.26	0.26	4
Fe I[f]	7.45	−2.00	0.13	75	−2.03	0.13	79	−2.25	0.11	75	−2.12	0.15	91	−2.03	0.13	78	−2.18	0.18	71	−2.02	0.17	67
Fe II[g]	7.45	−0.14	0.15	11	−0.10	0.14	11	0.07	0.21	9	−0.14	0.21	12	−0.06	0.19	6	−0.04	0.17	8	−0.14	0.26	6
Co I	4.92	0.11	0.06	2	0.25	0.10	2	0.01	···	1	0.09	0.06	5	0.19	0.16	3	0.05	···	1	···	···	···
Ni I	6.25	−0.01	0.18	16	−0.01	0.19	16	−0.06	0.16	11	−0.03	0.18	21	0.07	0.23	12	−0.06	0.22	13	−0.05	0.19	14
Cu I	4.21	−0.56	0.01	2	−0.53	0.17	2	−0.68	···	1	−0.71	0.02	2	−0.74	0.09	2	−0.61	···	1	−0.56	···	1
Zn I	4.60	−0.21	0.17	2	−0.15	0.08	2	···	···	···	−0.19	0.17	2	−0.32	0.02	2	···	···	···	···	···	···
Sr I	2.90	−0.86	···	1	−0.48	···	1	−0.48	···	1	···	···	···	−0.39	···	1	···	···	···	···	···	···
Sr II	2.90	···	···	···	···	···	···	−0.35	···	1	···	···	···	−0.25	···	1	···	···	···	···	···	···
Y II	2.24	−0.48	0.18	3	−0.56	0.13	5	−0.32	0.09	5	−0.36	0.24	4	−0.59	0.20	4	−0.44	0.08	3	−0.48	0.10	2
Zr I	2.60	···	···	···	···	···	···	···	···	···	0.49	···	1	···	···	···	···	···	···	···	···	···
Ba II	2.13	−0.25	0.10	4	−0.28	0.10	4	−0.05	0.16	3	0.16	0.24	3	−0.27	0.17	3	0.12	0.06	3	−0.05	0.17	3
La II	1.14	···	···	···	···	···	···	0.37	···	1	···	···	···	−0.26	···	1	···	···	···	···	···	···
Ce II	1.55	−0.23	0.09	2	−0.27	0.09	2	−0.16	0.05	2	···	···	···	−0.33	0.23	3	···	···	···	···	···	···
Nd II	1.50	0.12	0.01	2	−0.01	0.01	2	0.02	0.09	2	−0.15	0.16	4	−0.15	0.05	2	0.33	0.07	2	≤ 0.19	···	1
Eu II	0.51	0.25	0.15	2	0.32	0.08	2	0.30	0.11	2	0.33	0.16	2	0.05	0.20	2	≤0.84	···	1	···	···	···

[a] [X/Fe]: Fe I is used for neutral species, Fe II for ionized species.
[b] The rms dispersion about the mean of [X/Fe].
[c] From synthesis of the CH band near 4320 Å.
[d] The strong Na D lines are omitted.
[e] The strong Mg triplet lines are omitted.
[f] This is [Fe(Fe I)/H].
[g] This is [Fe(Fe II)/Fe(Fe I)]].

Table 2
W_λ for Five Mg-Poor Stars and S406 in NGC 2419 With Keck/HIRES Spectra

Line	Species	χ (eV)	$\log(gf)$ (dex)	S458 mÅ	S1004 mÅ	S1065 mÅ	S1131 mÅ	S1673 mÅ	S406 mÅ
5682.63	Na I	2.10	−0.700	18.6	17.3	···	13.0	28.6	15.7
5688.19	Na I	2.10	−0.420	23.0	28.1	27.5	36.0	53.2	38.5
5889.95	Na I	0.00	0.110	···	292.0	318.7	···	···	273.0
5895.92	Na I	0.00	−0.190	266.0	248.0	262.9	···	···	303.0
4703.00	Mg I	4.34	−0.440	73.3	75.4	48.0	56.0	28.4	130.2
5172.70	Mg I	2.71	−0.380	213.8	240.3	196.1	224.0	203.4	320.0
5183.62	Mg I	2.72	−0.160	249.0	275.0	232.5	266.0	228.0	390.0
5528.40	Mg I	4.34	−0.498	80.0	104.0	61.6	71.0	35.0	144.6
5711.09	Mg I	4.34	−1.724	···	···	···	15.5	···	31.6
6696.02	Al I	3.14	−1.340	10.0	15.0	≤10.0	−10.9	···	18.5
6698.67	Al I	3.14	−1.640	···	···	···	···	···	12.7
4102.94	Si I	1.91	−3.140	···	···	···	150.8	···	···
5665.55	Si I	4.92	−2.040	···	···	···	21.5	···	···
5690.43	Si I	4.93	−1.870	···	···	···	16.0	···	···
5772.15	Si I	5.08	−1.750	···	···	···	13.6	···	···
5948.54	Si I	5.08	−1.230	36.1	26.9	38.9	35.3	41.5	22.1
6155.13	Si I	5.62	−0.760	···	···	18.7	24.6	···	10.8
6237.32	Si I	5.62	−1.010	15.0	···	12.2	18.0	17.0	8.2
7003.57	Si I	5.96	−0.830	···	···	···	11.5	···	···
7005.89	Si I	5.98	−0.730	···	···	···	19.1	···	···
7034.90	Si I	5.87	−0.880	···	···	···	15.7	···	···
7405.77	Si I	5.61	−0.820	35.1	21.2	40.4	39.0	45.9	25.4
7415.95	Si I	5.61	−0.730	···	···	···	29.0	···	···
7423.50	Si I	5.62	−0.580	···	···	···	44.3	···	···
7698.97	K I	0.00	−0.168	162.1	160.6	163.0	175.0	210.8	119.7
4578.56	Ca I	2.52	−0.558	···	···	···	41.4	···	···
5512.99	Ca I	2.93	−0.300	···	···	···	32.3	···	···
5581.96	Ca I	2.52	−0.710	60.0	47.7	56.2	56.0	52.9	44.7
5588.75	Ca I	2.52	0.210	108.6	101.9	109.9	120.7	127.1	104.8
5590.11	Ca I	2.52	−0.710	49.2	62.5	55.9	57.2	60.2	52.5
5594.46	Ca I	2.52	−0.050	100.0	92.8	106.1	98.3	116.4	90.3
5601.28	Ca I	2.52	−0.690	68.0	58.3	58.2	67.3	54.0	48.6
5857.45	Ca I	2.93	0.230	75.2	79.8	81.1	87.2	94.2	74.0
6161.30	Ca I	2.52	−1.030	20.0	···	21.7	28.5	18.5	···
6162.17	Ca I	1.90	−0.090	150.8	151.9	156.4	164.7	···	145.0
6166.44	Ca I	2.52	−0.900	31.0	26.5	···	32.8	29.0	···
6169.04	Ca I	2.52	−0.540	50.0	47.0	51.3	47.2	45.7	38.5
6169.56	Ca I	2.52	−0.270	65.5	71.0	71.7	73.0	74.0	57.5
6471.66	Ca I	2.52	−0.590	54.5	66.9	57.7	62.0	67.9	51.2
6493.78	Ca I	2.52	0.140	93.0	97.6	103.0	101.8	107.8	87.7
6499.65	Ca I	2.54	−0.590	44.2	50.6	46.7	48.2	52.7	45.6
6717.68	Ca I	2.71	−0.610	52.5	63.6	61.1	62.9	58.3	···
7148.15	Ca I	2.71	0.218	99.0	100.9	112.2	112.4	137.3	99.8
5526.79	Sc II	1.77	0.130	113.7	110.7	122.8	122.0	153.9	82.8
5657.90	Sc II	1.51	−0.500	107.2	97.5	116.3	120.0	143.8	81.3
5667.15	Sc II	1.50	−1.240	58.5	60.9	73.5	54.1	84.2	···
5669.04	Sc II	1.50	−1.120	56.5	61.1	66.8	71.3	82.8	38.1
5684.20	Sc II	1.51	−1.080	45.7	72.5	78.0	73.1	113.5	54.7
6245.64	Sc II	1.51	−1.130	59.5	61.0	73.5	73.9	84.5	44.3
6604.59	Sc II	1.36	−1.310	54.0	51.0	70.6	66.1	76.5	34.4
4512.74	Ti I	0.84	−0.480	54.3	59.0	61.0	77.5	52.0	53.1
4533.25	Ti I	0.85	0.480	···	···	···	124.0	···	···
4534.78	Ti I	0.84	0.280	88.3	105.0	102.1	106.0	113.6	102.9
4548.77	Ti I	0.83	−0.350	55.3	69.6	65.0	75.3	63.8	71.1
4555.49	Ti I	0.85	−0.490	···	···	···	57.0	···	···
4681.92	Ti I	0.05	−1.070	80.3	96.8	101.5	100.4	102.8	104.6
4981.74	Ti I	0.85	0.500	118.4	120.6	120.8	133.8	127.6	130.9
4999.51	Ti I	0.83	0.250	98.3	102.1	123.4	119.2	124.6	112.8
5022.87	Ti I	0.83	−0.430	70.6	59.2	74.5	76.5	66.3	75.0
5039.96	Ti I	0.02	−1.130	93.7	84.5	108.6	104.1	99.0	102.4
5173.75	Ti I	0.00	−1.120	98.3	95.6	110.9	115.1	106.2	106.0
5210.39	Ti I	0.05	−0.880	107.5	107.9	116.8	126.3	···	121.8
5866.45	Ti I	1.07	−0.840	32.4	27.5	45.1	39.9	28.5	36.8
5922.11	Ti I	1.05	−1.470	···	···	20.9	17.3	···	14.2
5941.75	Ti I	1.05	−1.520	···	···	···	15.2	···	···
5953.16	Ti I	1.89	−0.329	···	···	···	20.6	···	···
5965.83	Ti I	1.88	−0.409	···	···	12.6	13.9	···	10.8
5978.54	Ti I	1.87	−0.496	···	···	···	12.8	···	···
6126.22	Ti I	1.07	−1.420	···	···	17.3	25.5	···	19.8
6258.10	Ti I	1.44	−0.355	26.9	···	33.1	39.0	23.4	···
6258.71	Ti I	1.46	−0.240	37.0	35.0	44.9	44.0	33.7	38.2
6261.10	Ti I	1.43	−0.479	25.0	22.7	33.1	38.4	···	30.8
6743.12	Ti I	0.90	−1.630	···	···	···	15.3	···	···
4399.77	Ti II	1.24	−1.290	···	···	···	151.0	···	···
4417.72	Ti II	1.16	−1.160	128.5	124.6	157.0	159.5	···	119.9
4583.41	Ti II	1.16	−2.870	50.7	49.5	59.1	69.1	53.4	···
4589.95	Ti II	1.24	−1.650	···	···	···	126.8	···	···
4657.20	Ti II	1.24	−2.320	···	···	···	90.0	···	···
4708.67	Ti II	1.24	−2.370	67.3	87.7	92.1	96.0	91.0	69.3
4865.62	Ti II	1.12	−2.810	75.4	63.5	71.2	74.5	78.0	58.3
4911.20	Ti II	3.12	−0.340	30.5	28.2	42.0	32.0	29.3	31.3
5185.91	Ti II	1.89	−1.460	85.4	79.8	84.2	86.0	100.5	77.2
6090.22	V I	1.08	−0.062	17.7	···	···	25.5	···	···
6199.20	V I	0.29	−1.280	···	···	···	21.5	···	···
6243.10	V I	0.30	−0.978	37.8	18.0	47.2	28.7	25.0	29.4
6251.82	V I	0.29	−1.340	···	···	16.0	10.6	···	···
4545.96	Cr I	0.94	−1.380	61.8	63.0	75.3	77.1	69.4	58.6
4600.76	Cr I	1.00	−1.280	···	···	···	75.4	···	···
4616.13	Cr I	0.98	−1.210	62.4	68.7	65.0	78.4	65.6	76.4
4626.18	Cr I	0.97	−1.340	65.8	66.1	69.7	81.8	59.1	64.9
5206.04	Cr I	0.94	0.030	149.0	155.0	···	···	175.1	···
5298.28	Cr I	0.98	−1.170	···	···	···	111.2	···	···
5409.80	Cr I	1.03	−0.710	116.0	115.0	130.7	132.7	119.1	128.3
4033.06	Mn I	0.00	−0.620	···	···	···	238.4	···	···
4754.04	Mn I	2.28	−0.090	82.7	60.1	89.5	80.2	61.1	72.7
4783.42	Mn I	2.30	0.042	79.5	67.0	84.5	84.1	75.1	78.6
4823.51	Mn I	2.32	0.140	80.0	79.1	85.1	94.7	80.6	92.6
5394.69	Mn I	0.00	−3.503	43.5	43.8	57.2	67.0	33.0	54.7
6021.80	Mn I	3.08	0.034	30.4	23.9	26.6	38.9	25.1	33.4
4602.95	Fe I	1.49	−2.220	125.4	115.0	139.3	148.3	148.3	139.1
4625.05	Fe I	3.24	−1.348	61.5	48.4	61.0	73.1	52.1	70.0
4788.77	Fe I	3.24	−1.806	35.7	27.2	···	31.5	···	···
4872.14	Fe I	2.88	−0.570	···	···	···	128.7	···	···
4891.50	Fe I	2.85	−0.110	138.6	···	147.5	152.5	157.3	150.4
4919.00	Fe I	2.86	−0.340	135.7	141.2	133.1	137.3	142.9	139.0
4920.51	Fe I	2.83	0.068	185.0	···	188.2	188.5	···	···

Table 2 — *Continued*

Line	Species	χ (eV)	$\log(gf)$ (dex)	S458 mÅ	S1004 mÅ	S1065 mÅ	S1131 mÅ	S1673 mÅ	S406 mÅ
5083.34	Fe I	0.96	−2.960	143.2	142.3	144.7	150.3	163.0	148.8
5166.28	Fe I	0.00	−4.200	150.0	159.8	161.8	163.1	165.4	163.8
5171.61	Fe I	1.48	−1.790	156.7	152.6	161.4	173.0	174.6	167.1
5192.35	Fe I	3.00	−0.420	124.9	129.1	123.0	···	140.2	131.1
5194.95	Fe I	1.56	−2.090	140.4	141.0	149.9	150.4	162.1	147.3
5198.72	Fe I	2.22	−2.140	98.1	96.2	96.5	104.3	98.0	101.3
5216.28	Fe I	1.61	−2.150	135.6	128.9	135.5	142.8	147.8	139.5
5217.40	Fe I	3.21	−1.070	71.3	69.2	79.1	77.0	70.0	78.0
5227.19	Fe I	1.56	−1.350	212.1	···	···	···	···	···
5232.95	Fe I	2.94	−0.100	141.0	142.9	147.6	159.4	158.8	145.6
5393.18	Fe I	3.24	−0.720	99.4	91.2	104.4	105.3	···	100.7
5410.92	Fe I	4.47	0.400	···	65.3	69.5	60.1	···	66.7
5415.21	Fe I	4.39	0.640	86.9	72.9	87.5	89.0	91.0	89.0
5424.08	Fe I	4.32	0.510	102.2	99.7	98.4	97.9	99.3	102.8
5445.05	Fe I	4.39	−0.030	58.1	67.4	63.0	65.8	46.0	68.8
5466.39	Fe I	4.37	−0.620	22.9	16.8	···	28.2	···	···
5473.90	Fe I	4.15	−0.690	28.7	···	21.5	27.2	···	34.9
5487.77	Fe I	4.14	−0.620	···	···	35.5	39.2	32.7	35.4
5497.52	Fe I	1.01	−2.830	171.7	153.1	172.3	···	···	167.8
5501.46	Fe I	0.96	−3.050	144.2	142.4	152.4	164.8	168.6	142.2
5506.79	Fe I	0.99	−2.790	159.1	152.5	171.6	···	175.7	165.4
5554.88	Fe I	4.55	−0.350	···	21.3	18.3	20.2	···	28.8
5567.39	Fe I	2.61	−2.670	30.5	···	33.5	44.9	···	30.9
5569.62	Fe I	3.42	−0.486	89.3	89.5	95.3	98.6	98.1	95.4
5572.84	Fe I	3.40	−0.275	115.9	111.5	114.6	115.4	119.2	112.3
5576.09	Fe I	3.43	−0.920	73.9	74.9	77.6	81.8	75.1	81.8
5586.76	Fe I	3.37	−0.140	116.9	106.3	120.2	131.0	129.9	124.4
5624.04	Fe I	4.39	−1.220	···	···	···	7.2	···	···
5624.54	Fe I	3.42	−0.755	84.0	78.2	87.1	86.9	84.3	86.8
5662.52	Fe I	4.18	−0.570	···	···	37.5	35.7	···	43.1
5701.54	Fe I	2.56	−2.140	60.9	57.5	68.4	69.5	63.3	65.1
5705.98	Fe I	4.61	−0.490	···	···	···	···	23.4	···
5753.12	Fe I	4.26	−0.690	27.6	24.7	23.7	19.2	17.9	21.3
5762.99	Fe I	4.21	−0.410	···	37.8	46.8	45.8	···	51.3
5775.06	Fe I	4.22	−1.300	···	10.1	···	14.9	···	···
5778.46	Fe I	2.59	−3.430	···	···	···	8.9	···	···
5806.72	Fe I	4.61	−0.950	···	···	···	8.9	···	···
5859.60	Fe I	4.55	−0.550	···	19.0	···	13.0	···	···
5862.35	Fe I	4.55	−0.330	25.9	···	23.1	24.1	···	28.5
5883.81	Fe I	3.96	−1.260	···	···	16.7	31.0	···	···
5930.17	Fe I	4.65	−0.140	23.3	23.0	26.2	28.5	30.0	28.2
5934.65	Fe I	3.93	−1.070	22.6	24.8	26.2	31.2	···	29.3
5952.72	Fe I	3.98	−1.340	···	···	···	17.8	···	···
5956.69	Fe I	0.86	−4.500	58.3	64.6	74.0	74.6	60.2	74.2
5976.79	Fe I	3.94	−1.330	···	···	···	24.2	···	···
5983.69	Fe I	4.55	−0.660	···	···	16.7	···	···	15.4
5984.83	Fe I	4.73	−0.260	···	···	20.8	···	···	18.2
6024.05	Fe I	4.55	0.030	···	47.5	46.9	54.6	···	50.5
6027.05	Fe I	4.07	−1.090	···	14.3	22.1	31.6	···	26.0
6055.99	Fe I	4.73	−0.370	···	13.2	12.6	21.7	···	15.8
6065.48	Fe I	2.61	−1.410	106.6	113.1	119.7	115.5	120.7	114.1
6078.50	Fe I	4.79	−0.330	···	···	···	13.5	···	14.1
6136.62	Fe I	2.45	−1.410	129.6	135.4	128.1	144.3	158.8	135.8
6136.99	Fe I	2.20	−2.930	57.1	57.4	69.5	···	···	44.5
6137.69	Fe I	2.59	−1.350	130.7	130.2	131.3	134.1	134.4	138.0
6151.62	Fe I	2.18	−3.370	30.5	27.9	33.1	36.4	26.0	35.8
6157.73	Fe I	4.07	−1.160	···	···	···	18.4	···	···
6165.36	Fe I	4.14	−1.470	···	···	···	6.2	···	···
6173.34	Fe I	2.22	−2.880	60.7	58.9	59.6	70.9	58.8	62.7
6180.20	Fe I	2.73	−2.650	31.4	30.4	30.1	33.1	23.4	34.4
6187.99	Fe I	3.94	−1.620	···	···	···	14.2	···	···
6191.56	Fe I	2.43	−1.420	126.1	123.1	135.9	140.9	128.0	141.8
6200.31	Fe I	2.61	−2.370	42.2	43.5	46.7	59.9	···	44.4
6240.65	Fe I	2.22	−3.170	···	28.9	38.2	33.2	24.7	35.6
6246.32	Fe I	3.60	−0.880	65.6	60.9	71.5	73.1	59.6	68.5
6252.55	Fe I	2.40	−1.770	118.1	120.4	127.3	127.5	121.5	125.0
6254.26	Fe I	2.28	−2.430	81.1	82.7	99.6	101.5	93.4	91.8
6265.13	Fe I	2.18	−2.540	83.8	84.2	96.0	95.5	87.4	87.9
6297.79	Fe I	2.22	−2.640	58.6	···	···	65.9	···	···
6301.51	Fe I	3.65	−0.718	58.2	···	···	73.6	···	···
6302.50	Fe I	3.69	−1.110	33.8	···	···	···	···	···
6315.31	Fe I	4.14	−1.230	···	···	···	10.4	···	···
6355.03	Fe I	2.84	−2.290	41.6	40.3	47.5	37.9	41.7	42.1
6380.75	Fe I	4.19	−1.380	···	···	···	11.6	···	···
6393.60	Fe I	2.43	−1.580	126.9	118.5	131.5	139.7	142.8	131.3
6408.03	Fe I	3.69	−1.020	35.3	27.5	43.6	53.2	···	58.6
6411.65	Fe I	3.65	−0.720	66.1	56.8	73.4	78.3	···	94.3
6430.84	Fe I	2.18	−1.950	119.3	121.2	129.3	132.6	131.2	132.0
6475.63	Fe I	2.56	−2.940	27.7	25.0	35.1	···	23.3	33.7
6481.87	Fe I	2.28	−3.010	47.9	45.4	50.7	55.2	37.8	55.8
6494.98	Fe I	2.40	−1.240	146.2	143.7	155.5	152.3	162.2	146.2
6498.94	Fe I	0.96	−4.690	55.6	41.9	64.3	68.4	50.0	65.4
6546.24	Fe I	2.76	−1.540	92.6	94.5	94.5	104.0	93.2	97.7
6592.91	Fe I	2.73	−1.470	101.5	97.9	110.4	117.5	107.0	105.9
6593.87	Fe I	2.43	−2.370	70.4	70.9	82.7	84.2	70.0	84.4
6609.11	Fe I	2.56	−2.660	40.7	36.1	41.9	43.3	···	45.9
6625.02	Fe I	1.01	−5.370	···	12.3	···	22.5	···	···
6648.12	Fe I	1.01	−5.920	···	···	···	7.7	···	···
6703.57	Fe I	2.76	−3.060	···	11.6	18.5	16.2	···	···
6739.52	Fe I	1.56	−4.790	···	···	10.5	···	···	···
6750.15	Fe I	2.42	−2.580	61.4	58.9	76.3	77.0	67.9	67.8
6839.83	Fe I	2.56	−3.350	···	···	···	12.3	···	···
6855.18	Fe I	4.56	−0.740	15.4	···	15.0	13.8	···	14.5
6861.95	Fe I	2.42	−3.850	···	···	···	8.9	···	···
6978.85	Fe I	2.48	−2.450	···	···	···	73.3	···	···
6988.52	Fe I	2.40	−3.560	···	···	···	20.3	···	···
6999.88	Fe I	4.10	−1.460	···	···	···	11.6	···	···
7022.95	Fe I	4.19	−1.150	···	···	···	15.6	···	···
7038.22	Fe I	4.22	−1.200	···	···	···	22.0	···	···
7130.92	Fe I	4.22	−0.750	···	···	···	34.0	···	···
7151.47	Fe I	2.48	−3.660	···	···	···	8.6	···	···
7179.99	Fe I	1.48	−4.750	···	···	···	11.2	···	···
7288.74	Fe I	4.22	−1.280	···	···	···	18.3	···	···
7411.16	Fe I	4.28	−0.280	35.4	36.8	36.4	···	46.2	42.7
7418.67	Fe I	4.14	−1.380	···	···	···	10.1	···	···
7445.75	Fe I	4.26	0.030	51.9	51.6	61.8	57.6	52.0	61.3
7568.91	Fe I	4.28	−0.940	···	···	···	21.9	···	···

Table 2 — *Continued*

Line	Species	χ (eV)	$\log(gf)$ (dex)	S458 mÅ	S1004 mÅ	S1065 mÅ	S1131 mÅ	S1673 mÅ	S406 mÅ
7583.79	Fe I	3.02	−1.890	47.7	46.2	61.4	56.3	47.7	58.0
7586.04	Fe I	4.31	−0.130	40.9	43.4	47.9	56.7	···	56.9
7742.72	Fe I	4.99	−0.420	···	···	···	21.2	···	···
7748.27	Fe I	2.95	−1.750	60.6	71.0	80.8	83.6	75.5	78.1
7780.57	Fe I	4.47	−0.040	35.5	45.3	41.6	45.4	40.3	39.7
4508.30	Fe II	2.84	−2.280	74.1	77.0	87.3	83.1	···	86.6
4576.34	Fe II	2.83	−2.900	49.3	56.9	59.0	60.0	···	58.4
4923.93	Fe II	2.88	−1.320	143.3	127.0	136.8	146.0	···	141.4
5018.45	Fe II	2.89	−1.220	164.4	···	164.8	167.6	···	160.8
5197.58	Fe II	3.23	−2.230	69.8	82.0	70.6	76.8	95.3	72.7
5234.63	Fe II	3.22	−2.220	75.0	78.4	73.7	80.8	95.5	69.2
5425.26	Fe II	3.00	−3.240	21.7	···	40.1	24.3	29.8	21.8
5534.85	Fe II	3.25	−2.640	28.7	49.7	50.7	42.4	···	40.1
5991.38	Fe II	3.15	−3.570	25.5	···	···	···	···	···
6149.26	Fe II	3.89	−2.690	···	17.4	18.3	12.2	···	16.9
6247.56	Fe II	3.89	−2.360	30.5	40.0	22.1	25.5	···	27.5
6456.39	Fe II	3.90	−2.310	39.0	45.6	···	···	57.0	···
6516.08	Fe II	2.89	−3.450	39.9	39.3	48.1	42.3	···	40.3
5483.34	Co I	1.71	−1.490	23.9	33.2	47.7	36.0	32.6	40.8
6814.94	Co I	1.96	−1.900	···	18.6	12.2	16.0	···	16.8
7417.41	Co I	2.04	−2.070	···	···	···	6.0	···	···
5578.72	Ni I	1.68	−2.640	36.7	···	49.0	51.6	33.6	40.3
5587.86	Ni I	1.93	−2.140	33.1	29.2	44.2	···	29.9	44.8
5592.26	Ni I	1.95	−2.590	42.9	32.0	36.9	48.4	35.0	35.5
5748.35	Ni I	1.68	−3.260	···	10.6	24.5	20.2	15.2	21.3
5846.99	Ni I	1.68	−3.210	···	···	···	17.4	···	···
5892.87	Ni I	1.99	−2.340	48.8	59.5	60.5	66.5	42.7	59.7
6128.97	Ni I	1.68	−3.330	···	···	···	18.2	···	···
6314.66	Ni I	1.93	−1.770	45.2	···	···	···	···	···
6482.80	Ni I	1.93	−2.630	14.2	20.5	20.5	22.1	14.3	52.4
6586.31	Ni I	1.95	−2.810	23.0	20.4	29.9	26.6	14.7	24.5
6643.63	Ni I	1.68	−2.300	78.4	79.0	91.0	94.0	80.4	99.3
6767.77	Ni I	1.83	−2.170	72.3	68.2	83.1	83.2	75.6	78.9
7122.20	Ni I	3.54	0.048	59.0	47.6	65.8	65.8	53.5	66.1
7414.50	Ni I	1.99	−2.570	36.1	30.1	53.9	48.7	33.1	44.5
7422.27	Ni I	3.63	−0.129	38.6	32.1	41.6	53.2	40.5	43.3
7574.05	Ni I	3.83	−0.580	12.2	23.1	16.0	20.6	20.7	16.2
7727.62	Ni I	3.68	−0.162	29.5	43.1	38.4	47.9	36.0	41.8
7748.89	Ni I	3.70	−0.130	···	···	···	41.9	···	···
7788.93	Ni I	1.95	−2.420	68.6	62.2	73.2	79.0	55.9	70.6
7797.59	Ni I	3.90	−0.180	28.1	29.1	23.6	26.6	···	25.9
5105.54	Cu I	1.39	−1.505	36.3	35.7	49.5	43.1	33.4	39.0
5782.12	Cu I	1.64	−1.780	···	22.6	···	···	···	24.6
4722.16	Zn I	4.03	−0.390	38.0	36.0	33.6	39.0	56.7	37.0
4810.54	Zn I	4.08	−0.170	41.2	46.6	41.3	39.0	48.1	40.1
4607.33	Sr I	0.00	0.280	···	···	13.5	22.7	···	16.7
4554.04	Ba II	0.00	0.170	···	···	194.4	213.2	···	188.1
5853.70	Ba II	0.60	−1.010	79.3	74.2	81.1	103.2	104.7	76.8
6141.70	Ba II	0.70	−0.070	125.9	144.1	136.4	149.1	174.9	135.9
6496.90	Ba II	0.60	−0.380	139.2	140.3	138.7	147.7	178.0	133.8
4883.69	Y II	1.08	0.070	61.5	72.9	60.3	68.6	74.8	58.1
5087.43	Y II	1.08	−0.170	38.9	45.0	46.1	52.8	61.9	40.5
5123.22	Y II	0.99	−0.830	···	···	24.2	···	34.7	27.0
5200.42	Y II	0.99	−0.570	38.0	34.5	34.7	45.9	···	25.0
5205.73	Y II	1.03	−0.340	64.1	···	38.8	···	···	40.6
6390.48	La II	0.32	−1.410	···	···	···	8.1	···	···
4486.91	Ce II	0.30	−0.360	···	···	···	25.5	···	···
4562.37	Ce II	0.48	0.330	19.3	24.1	18.8	40.5	···	32.8
4628.16	Ce II	0.52	0.260	25.5	34.3	27.0	30.6	21.0	21.5
4446.39	Nd II	0.20	−0.350	···	···	···	24.8	···	···
4959.12	Nd II	0.06	−0.800	···	36.0	24.2	42.0	23.0	24.1
5092.79	Nd II	0.38	−0.610	···	···	···	14.2	···	···
5212.35	Nd II	0.20	−0.960	···	···	···	11.2	···	···
5249.58	Nd II	0.98	0.200	···	25.9	20.9	19.5	18.4	17.5
4129.70	Eu II	0.00	0.220	135.0	127.7	74.1	125.0	116.9	128.3
6645.11	Eu II	1.38	0.120	16.6	···	···	17.0	···	10.0

Table 3
W_λ for 7 Mg-Normal RGB Stars in NGC 2419 With Keck/HIRES Spectra

Line	Species	χ (eV)	$\log(gf)$ (dex)	S810 mÅ	S973 mÅ	S1166 mÅ	S1209 mÅ	S1305 mÅ	S1814 mÅ	S223 mÅ
6300.30	[O I]	0.00	−9.780	21.0	54.7	···	36.7	···	···	···
6363.78	[O I]	0.02	−10.300	14.3	23.5	···	···	···	···	···
5682.63	Na I	2.10	−0.700	6.0	···	···	···	···	30.3	30.3
5688.19	Na I	2.10	−0.420	15.0	···	20.3	···	···	46.0	46.0
5889.95	Na I	0.00	0.110	···	362.0	270.0	···	376.0	···	···
5895.92	Na I	0.00	−0.190	236.0	279.0	304.0	282.0	355.0	···	···
4703.00	Mg I	4.34	−0.440	107.0	123.0	116.5	125.0	102.3	92.0	92.0
5172.70	Mg I	2.71	−0.380	330.0	345.0	346.5	311.0	312.2	340.0	340.0
5183.62	Mg I	2.72	−0.160	395.0	396.0	405.5	398.0	365.6	406.8	406.8
5528.40	Mg I	4.34	−0.498	135.0	122.2	156.6	139.2	120.9	140.0	140.0
5711.09	Mg I	4.34	−1.724	44.5	73.0	57.8	43.3	40.8	44.0	44.0
6696.02	Al I	3.14	−1.340	7.5	···	···	···	···	18.0	18.0
5948.54	Si I	5.08	−1.230	···	15.0	35.2	···	20.3	21.8	21.8
6155.13	Si I	5.62	−0.760	···	···	18.5	···	···	···	···
7005.89	Si I	5.98	−0.730	···	···	···	···	15.5	···	···
7405.77	Si I	5.61	−0.820	···	···	21.0	···	···	28.8	28.8
7415.95	Si I	5.61	−0.730	···	···	···	···	25.4	16.0	16.0
7423.50	Si I	5.62	−0.580	···	40.1	···	···	32.7	26.3	26.3
7698.97	K I	0.00	−0.168	129.1	104.2	134.6	114.6	108.3	151.6	151.6
5512.99	Ca I	2.93	−0.300	···	24.0	···	···	···	···	···
5581.96	Ca I	2.52	−0.710	···	50.9	50.5	35.0	47.2	48.6	48.6
5588.75	Ca I	2.52	0.210	93.5	109.7	107.9	98.2	79.0	111.7	111.7
5590.11	Ca I	2.52	−0.710	47.2	57.2	61.4	47.0	41.2	47.7	47.7
5594.46	Ca I	2.52	−0.050	···	···	103.3	85.2	94.0	···	···
5601.28	Ca I	2.52	−0.690	54.3	50.3	57.8	42.0	···	53.8	53.8
5857.45	Ca I	2.93	0.230	72.4	90.0	73.1	69.2	62.3	76.6	76.6
6161.30	Ca I	2.52	−1.030	19.9	32.4	···	19.0	···	24.7	24.7
6162.17	Ca I	1.90	−0.090	150.9	160.9	160.5	147.0	145.0	···	···
6166.44	Ca I	2.52	−0.900	···	22.1	23.6	24.2	18.0	25.9	25.9
6169.04	Ca I	2.52	−0.540	50.6	63.0	56.6	39.2	45.3	58.0	58.0
6169.56	Ca I	2.52	−0.270	67.4	64.0	63.2	56.8	52.0	59.9	59.9
6471.66	Ca I	2.52	−0.590	52.9	54.2	55.1	39.7	53.1	52.8	52.8
6493.78	Ca I	2.52	0.140	89.9	111.2	95.4	91.3	90.4	95.7	95.7
6499.65	Ca I	2.54	−0.590	47.3	···	48.5	···	40.0	38.2	38.2
6717.68	Ca I	2.71	−0.610	···	61.2	56.0	44.9	55.6	55.3	55.3
7148.15	Ca I	2.71	0.218	···	130.2	109.3	···	101.8	111.3	111.3
5526.79	Sc II	1.77	0.130	86.1	75.0	87.8	78.4	80.8	111.0	111.0
5657.90	Sc II	1.51	−0.500	79.3	75.7	81.8	80.9	64.9	99.8	99.8
5667.15	Sc II	1.50	−1.240	31.7	34.0	44.2	34.5	34.2	43.2	43.2
5669.04	Sc II	1.50	−1.120	35.2	40.6	41.8	···	50.8	43.7	43.7
5684.20	Sc II	1.51	−1.080	49.0	42.1	51.5	47.2	29.9	54.7	54.7
6245.64	Sc II	1.51	−1.130	49.4	48.4	47.9	41.3	46.9	55.6	55.6
6604.59	Sc II	1.36	−1.310	43.5	53.0	43.9	38.8	43.1	42.0	42.0
4512.74	Ti I	0.84	−0.480	···	···	72.6	53.4	···	75.4	75.4
4518.03	Ti I	0.83	−0.230	···	···	···	69.0	···	···	···
4533.25	Ti I	0.85	0.480	101.7	···	···	107.4	···	···	···
4534.78	Ti I	0.84	0.280	97.8	···	118.5	81.0	···	129.7	129.7
4548.77	Ti I	0.83	−0.350	57.9	···	86.1	78.5	···	94.0	94.0
4555.49	Ti I	0.85	−0.490	···	···	···	46.7	···	···	···
4681.92	Ti I	0.05	−1.070	110.5	···	106.4	111.6	···	···	···
4981.74	Ti I	0.85	0.500	136.6	···	129.1	115.2	···	···	···
4999.51	Ti I	0.83	0.250	111.4	139.4	127.4	115.1	107.1	152.8	152.8
5022.87	Ti I	0.83	−0.430	81.2	114.0	83.0	77.2	74.4	99.3	99.3
5039.96	Ti I	0.02	−1.130	118.7	108.0	120.3	111.0	95.8	163.1	163.1
5173.75	Ti I	0.00	−1.120	120.3	133.8	129.4	114.3	112.0	157.6	157.6
5210.39	Ti I	0.05	−0.880	142.5	147.0	142.5	123.3	143.0	···	···
5426.26	Ti I	0.02	−3.010	···	···	···	···	···	30.2	30.2
5490.15	Ti I	1.46	−0.933	···	···	···	···	···	10.5	10.5
5866.45	Ti I	1.07	−0.840	51.9	38.7	58.0	27.6	32.4	56.9	56.9
5922.11	Ti I	1.05	−1.470	···	···	···	···	···	31.1	31.1
5941.75	Ti I	1.05	−1.520	···	···	···	···	···	15.8	15.8
5953.16	Ti I	1.89	−0.329	···	···	···	···	···	19.5	19.5
5965.83	Ti I	1.88	−0.409	18.0	···	···	···	···	18.6	18.6
6126.22	Ti I	1.07	−1.420	···	···	29.1	15.7	23.0	30.0	30.0
6258.10	Ti I	1.44	−0.355	46.2	···	46.4	26.2	31.0	47.0	47.0
6258.71	Ti I	1.46	−0.240	52.1	42.2	60.4	31.2	34.4	61.1	61.1
6261.10	Ti I	1.43	−0.479	···	32.6	47.0	···	30.6	44.4	44.4
6743.12	Ti I	0.90	−1.630	···	16.8	···	···	···	21.5	21.5
4417.72	Ti II	1.16	−1.160	···	···	132.0	···	···	···	···
4501.28	Ti II	1.12	−0.760	149.4	···	···	173.4	···	···	···
4563.77	Ti II	1.22	−0.820	134.4	···	···	164.1	···	···	···
4571.98	Ti II	1.57	−0.340	161.1	···	···	173.7	···	···	···
4583.41	Ti II	1.16	−2.870	···	···	52.5	49.2	···	···	···
4589.95	Ti II	1.24	−1.650	99.1	···	···	116.2	···	134.0	134.0
4657.20	Ti II	1.24	−2.320	78.4	···	···	80.7	···	···	···
4708.67	Ti II	1.24	−2.370	···	58.0	78.5	83.0	69.0	74.3	74.3
4762.78	Ti II	1.08	−2.710	···	···	···	83.0	···	···	···
4798.54	Ti II	1.08	−2.670	···	···	···	···	65.4	···	···
4865.62	Ti II	1.12	−2.810	···	62.0	60.9	···	59.0	68.1	68.1
4911.20	Ti II	3.12	−0.340	25.0	27.5	27.7	48.0	21.8	30.0	30.0
5185.91	Ti II	1.89	−1.460	74.1	83.0	82.2	76.9	89.0	104.2	104.2
5670.85	V I	1.08	−0.425	···	···	···	···	···	22.0	22.0
5703.57	V I	1.05	−0.212	21.7	···	···	17.1	···	17.0	17.0
6081.44	V I	1.05	−0.579	···	···	···	···	···	10.3	10.3
6090.22	V I	1.08	−0.062	24.9	29.9	20.9	20.8	···	24.3	24.3
6199.20	V I	0.29	−1.280	···	···	···	···	···	29.9	29.9
6243.10	V I	0.30	−0.978	49.1	49.3	44.3	22.9	16.9	33.1	33.1
6251.82	V I	0.29	−1.340	···	21.0	17.3	···	···	18.0	18.0
6274.64	V I	0.27	−1.670	···	···	···	···	···	10.7	10.7
6285.14	V I	0.28	−1.510	···	···	21.2	···	16.9	19.1	19.1
4545.96	Cr I	0.94	−1.380	69.2	···	67.4	58.6	···	86.9	86.9
4600.76	Cr I	1.00	−1.280	···	···	···	73.0	···	···	···
4616.13	Cr I	0.98	−1.210	···	···	91.2	···	···	88.4	88.4
4626.18	Cr I	0.97	−1.340	67.4	···	70.4	57.0	···	92.5	92.5
4652.17	Cr I	1.00	−1.030	89.7	···	···	79.2	···	98.2	98.2
5206.04	Cr I	0.94	0.030	···	175.0	···	174.0	139.8	···	···
5409.80	Cr I	1.03	−0.710	131.4	131.8	143.2	111.8	108.5	169.0	169.0
4754.04	Mn I	2.28	−0.090	75.8	77.8	92.8	83.5	63.6	74.1	74.1
4783.42	Mn I	2.30	0.042	91.6	91.4	86.1	81.4	79.8	96.6	96.6
4823.51	Mn I	2.32	0.140	87.3	118.0	98.2	82.7	88.0	99.5	99.5
5394.69	Mn I	0.00	−3.503	88.8	84.2	89.7	57.9	42.5	101.0	101.0
6013.50	Mn I	3.07	−0.252	13.5	···	···	9.9	···	···	···
6021.80	Mn I	3.08	0.034	37.4	···	36.5	27.2	28.0	36.3	36.3
4489.75	Fe I	0.12	−3.970	146.3	···	···	···	···	···	···
4494.57	Fe I	2.20	−1.140	···	···	···	142.6	···	···	···
4531.16	Fe I	1.49	−2.150	147.8	···	···	126.7	···	···	···

Table 3 — *Continued*

Line	Species	χ (eV)	$\log(gf)$ (dex)	S810 mÅ	S973 mÅ	S1166 mÅ	S1209 mÅ	S1305 mÅ	S1814 mÅ	S223 mÅ
4602.95	Fe I	1.49	−2.220	129.3	···	152.2	137.3	···	···	···
4625.05	Fe I	3.24	−1.348	57.8	···	71.0	50.7	···	75.6	75.6
4788.77	Fe I	3.24	−1.806	35.9	···	42.1	···	···	34.1	34.1
4871.33	Fe I	2.86	−0.360	127.9	···	···	126.3	···	···	···
4891.50	Fe I	2.85	−0.110	149.4	···	151.1	147.3	···	···	···
4919.00	Fe I	2.86	−0.340	137.6	136.0	143.0	135.0	···	161.9	161.9
5083.34	Fe I	0.96	−2.960	143.7	157.1	158.1	150.6	141.9	···	···
5166.28	Fe I	0.00	−4.200	174.0	···	···	179.9	167.6	···	···
5171.61	Fe I	1.48	−1.790	157.0	175.5	···	170.6	···	···	···
5192.35	Fe I	3.00	−0.420	122.2	116.0	136.4	126.3	109.0	157.0	157.0
5194.95	Fe I	1.56	−2.090	154.9	159.4	159.8	159.5	152.9	···	···
5198.72	Fe I	2.22	−2.140	103.4	97.9	105.3	95.8	95.2	128.3	128.3
5216.28	Fe I	1.61	−2.150	155.4	···	145.5	137.1	133.0	···	···
5217.40	Fe I	3.21	−1.070	···	102.0	78.3	···	68.2	78.9	78.9
5232.95	Fe I	2.94	−0.100	145.2	168.6	145.0	141.1	139.6	···	···
5393.18	Fe I	3.24	−0.720	105.2	131.0	103.5	87.4	84.1	114.5	114.5
5410.92	Fe I	4.47	0.400	56.9	69.6	77.8	62.7	46.2	71.2	71.2
5415.21	Fe I	4.39	0.640	84.2	79.1	96.8	78.3	73.3	85.7	85.7
5424.08	Fe I	4.32	0.510	89.9	82.6	103.4	85.9	86.0	107.8	107.8
5445.05	Fe I	4.39	−0.030	···	···	71.7	51.1	41.1	56.6	56.6
5466.39	Fe I	4.37	−0.620	25.5	···	29.7	20.6	···	25.0	25.0
5473.90	Fe I	4.15	−0.690	30.1	34.5	29.2	24.3	25.6	23.7	23.7
5487.77	Fe I	4.14	−0.620	38.8	59.2	42.2	26.3	···	31.5	31.5
5497.52	Fe I	1.01	−2.830	174.3	170.3	···	164.2	165.1	···	···
5501.46	Fe I	0.96	−3.050	161.6	152.2	173.5	155.1	147.9	···	···
5506.79	Fe I	0.99	−2.790	···	168.1	···	167.1	158.9	···	···
5522.45	Fe I	4.21	−1.450	7.2	···	···	···	···	···	···
5554.88	Fe I	4.55	−0.350	29.6	···	35.0	17.9	···	16.7	16.7
5567.39	Fe I	2.61	−2.670	42.2	···	···	39.2	29.9	49.8	49.8
5569.62	Fe I	3.42	−0.486	99.4	92.4	103.2	87.5	80.0	106.7	106.7
5572.84	Fe I	3.40	−0.275	116.3	···	120.0	111.2	108.8	129.1	129.1
5576.09	Fe I	3.43	−0.920	82.5	80.3	86.1	69.9	74.9	90.1	90.1
5586.76	Fe I	3.37	−0.140	120.5	125.3	132.9	120.8	122.0	143.8	143.8
5624.54	Fe I	3.42	−0.755	86.2	103.2	93.8	72.4	68.0	100.4	100.4
5641.44	Fe I	4.26	−1.080	···	22.3	···	···	···	···	···
5662.52	Fe I	4.18	−0.570	37.4	···	46.8	41.4	29.7	···	···
5701.54	Fe I	2.56	−2.140	78.1	68.7	78.2	64.9	72.4	83.8	83.8
5705.98	Fe I	4.61	−0.490	···	···	···	···	···	16.1	16.1
5753.12	Fe I	4.26	−0.690	26.8	···	30.5	15.2	···	26.6	26.6
5762.99	Fe I	4.21	−0.410	48.6	47.3	53.8	28.9	47.6	40.6	40.6
5778.46	Fe I	2.59	−3.430	···	···	···	···	···	9.3	9.3
5859.60	Fe I	4.55	−0.550	···	···	···	···	···	13.3	13.3
5862.35	Fe I	4.55	−0.330	···	32.1	21.3	···	23.7	25.6	25.6
5883.81	Fe I	3.96	−1.260	···	···	18.0	···	···	26.7	26.7
5930.17	Fe I	4.65	−0.140	30.4	26.0	···	21.7	40.6	36.0	36.0
5934.65	Fe I	3.93	−1.070	29.3	···	31.3	21.9	···	34.2	34.2
5952.72	Fe I	3.98	−1.340	···	···	···	···	···	14.2	14.2
5956.69	Fe I	0.86	−4.500	89.8	94.3	91.0	75.9	80.0	99.8	99.8
5976.79	Fe I	3.94	−1.330	26.5	33.4	···	···	···	22.5	22.5
5983.69	Fe I	4.55	−0.660	10.1	···	17.1	···	···	19.6	19.6
6024.05	Fe I	4.55	0.030	53.0	45.7	61.8	45.3	41.1	56.5	56.5
6027.05	Fe I	4.07	−1.090	36.3	···	25.0	16.9	19.1	24.9	24.9
6055.99	Fe I	4.73	−0.370	···	···	18.5	···	···	16.1	16.1
6065.48	Fe I	2.61	−1.410	125.3	131.7	127.7	115.0	105.6	141.4	141.4
6078.50	Fe I	4.79	−0.330	···	···	···	···	17.8	···	···
6136.62	Fe I	2.45	−1.410	145.4	139.4	148.1	136.5	114.1	···	···
6136.99	Fe I	2.20	−2.930	···	···	89.4	···	54.2	···	···
6137.69	Fe I	2.59	−1.350	139.8	132.1	147.9	128.2	126.5	159.4	159.4
6151.62	Fe I	2.18	−3.370	45.0	47.0	48.6	33.3	22.9	48.8	48.8
6157.73	Fe I	4.07	−1.160	···	34.8	···	···	···	16.4	16.4
6173.34	Fe I	2.22	−2.880	80.8	65.1	77.2	65.3	59.6	87.0	87.0
6180.20	Fe I	2.73	−2.650	34.3	43.0	···	21.5	26.8	40.7	40.7
6191.56	Fe I	2.43	−1.420	145.1	143.4	148.3	135.2	121.7	150.3	150.3
6200.31	Fe I	2.61	−2.370	63.3	86.4	60.3	44.6	56.1	71.5	71.5
6240.65	Fe I	2.22	−3.170	52.7	42.6	50.8	32.1	29.4	47.2	47.2
6246.32	Fe I	3.60	−0.880	69.8	71.8	78.0	60.2	72.3	76.8	76.8
6252.55	Fe I	2.40	−1.770	122.8	118.8	133.7	119.2	116.8	148.6	148.6
6254.26	Fe I	2.28	−2.430	97.3	93.5	102.2	85.8	80.6	113.9	113.9
6265.13	Fe I	2.18	−2.540	106.3	122.0	105.1	89.2	83.3	111.9	111.9
6297.79	Fe I	2.22	−2.640	77.1	85.3	···	62.5	66.7	92.6	92.6
6301.51	Fe I	3.65	−0.718	72.1	···	···	61.9	61.6	76.3	76.3
6302.50	Fe I	3.69	−1.110	43.3	56.7	···	···	···	51.3	51.3
6311.50	Fe I	2.83	−3.140	···	···	···	···	···	13.6	13.6
6315.81	Fe I	4.07	−1.610	10.8	···	···	···	···	···	···
6355.03	Fe I	2.84	−2.290	56.2	39.3	54.8	37.1	39.5	45.7	45.7
6380.75	Fe I	4.19	−1.380	···	···	···	···	···	10.6	10.6
6393.60	Fe I	2.43	−1.580	141.0	139.1	142.5	127.2	133.9	162.0	162.0
6408.03	Fe I	3.69	−1.020	53.5	63.8	57.2	45.4	53.8	50.7	50.7
6411.65	Fe I	3.65	−0.720	77.9	86.8	80.7	72.2	78.7	85.9	85.9
6421.35	Fe I	2.28	−2.010	···	···	···	120.3	···	···	···
6430.84	Fe I	2.18	−1.950	128.8	141.9	138.8	129.6	134.9	165.6	165.6
6475.63	Fe I	2.56	−2.940	41.7	···	43.3	26.0	···	49.5	49.5
6481.87	Fe I	2.28	−3.010	63.3	65.6	66.1	46.5	42.3	72.7	72.7
6494.98	Fe I	2.40	−1.240	159.2	166.6	166.0	153.1	149.0	···	···
6498.94	Fe I	0.96	−4.690	83.2	79.0	84.6	60.6	64.3	88.4	88.4
6546.24	Fe I	2.76	−1.540	108.5	122.0	110.9	95.8	89.8	125.0	125.0
6581.21	Fe I	1.48	−4.680	···	···	···	···	11.3	16.6	16.6
6592.91	Fe I	2.73	−1.470	119.3	117.7	119.4	111.4	102.3	127.1	127.1
6593.87	Fe I	2.43	−2.370	86.8	93.8	89.8	71.9	80.1	96.1	96.1
6608.02	Fe I	2.28	−3.930	11.1	···	···	8.4	···	···	···
6609.11	Fe I	2.56	−2.660	63.0	54.1	57.8	47.0	44.6	54.9	54.9
6625.02	Fe I	1.01	−5.370	33.6	23.0	33.7	23.0	···	38.0	38.0
6648.12	Fe I	1.01	−5.920	···	···	···	···	···	11.9	11.9
6703.57	Fe I	2.76	−3.060	···	···	32.7	···	18.0	19.4	19.4
6739.52	Fe I	1.56	−4.790	21.8	···	13.3	···	···	···	···
6750.15	Fe I	2.42	−2.580	81.3	87.2	83.5	68.4	63.2	90.9	90.9
6839.83	Fe I	2.56	−3.350	···	···	···	···	···	12.3	12.3
6855.18	Fe I	4.56	−0.740	···	···	···	···	···	17.9	17.9
6978.85	Fe I	2.48	−2.450	···	93.6	···	···	65.8	96.4	96.4
6988.52	Fe I	2.40	−3.560	···	···	···	···	···	20.4	20.4
6999.88	Fe I	4.10	−1.460	···	···	···	···	···	13.8	13.8
7022.95	Fe I	4.19	−1.150	···	···	···	···	···	20.5	20.5
7112.17	Fe I	2.99	−3.100	···	···	···	···	···	12.4	12.4
7130.92	Fe I	4.22	−0.750	···	26.2	···	···	28.8	29.4	29.4
7151.47	Fe I	2.48	−3.660	···	···	···	···	···	19.3	19.3
7179.99	Fe I	1.48	−4.750	···	···	···	···	···	28.4	28.4
7411.16	Fe I	4.28	−0.280	···	69.3	44.9	···	31.6	40.0	40.0

Table 3 — *Continued*

Line	Species	χ (eV)	$\log(gf)$ (dex)	S810 mÅ	S973 mÅ	S1166 mÅ	S1209 mÅ	S1305 mÅ	S1814 mÅ	S223 mÅ
7445.75	Fe I	4.26	0.030	···	65.0	73.5	···	57.6	65.8	65.8
7461.52	Fe I	2.56	−3.530	···	···	···	···	···	22.8	22.8
7568.91	Fe I	4.28	−0.940	···	···	···	···	···	24.7	24.7
7583.79	Fe I	3.02	−1.890	···	71.5	65.4	···	50.4	67.2	67.2
7586.04	Fe I	4.31	−0.130	···	63.8	57.3	···	40.0	48.0	48.0
7748.27	Fe I	2.95	−1.750	···	105.0	96.8	···	76.2	102.9	102.9
7780.57	Fe I	4.47	−0.040	···	54.5	53.8	···	37.0	62.9	62.9
4416.82	Fe II	2.77	−2.430	···	···	···	···	···	61.0	61.0
4491.40	Fe II	2.84	−2.600	···	···	···	70.7	···	71.0	71.0
4508.30	Fe II	2.84	−2.280	···	···	81.5	73.1	···	86.4	86.4
4555.89	Fe II	2.82	−2.170	···	···	···	100.2	···	···	···
4576.34	Fe II	2.83	−2.900	···	···	61.8	···	···	46.0	46.0
4583.84	Fe II	2.81	−2.020	98.0	···	···	···	···	···	···
4923.93	Fe II	2.88	−1.320	127.3	132.4	133.1	142.9	123.6	157.0	157.0
5018.45	Fe II	2.89	−1.220	146.9	···	165.6	155.0	146.0	···	···
5197.58	Fe II	3.23	−2.230	65.1	78.6	69.3	60.6	61.2	84.1	84.1
5234.63	Fe II	3.22	−2.220	73.0	58.8	68.0	62.3	72.5	82.3	82.3
5425.26	Fe II	3.00	−3.240	···	17.0	24.8	···	20.0	24.8	24.8
5534.85	Fe II	3.25	−2.640	···	···	46.8	···	45.2	35.0	35.0
6149.26	Fe II	3.89	−2.690	···	···	13.7	···	···	11.2	11.2
6247.56	Fe II	3.89	−2.360	···	37.0	24.3	···	20.0	27.7	27.7
6456.39	Fe II	3.90	−2.310	46.4	···	···	38.1	···	···	···
6516.08	Fe II	2.89	−3.450	···	35.6	39.6	29.1	40.7	33.9	33.9
5483.34	Co I	1.71	−1.490	58.7	···	55.2	30.1	29.4	···	···
5530.79	Co I	1.71	−2.060	27.2	···	···	···	···	18.0	18.0
6189.00	Co I	1.71	−2.450	···	···	···	···	···	9.5	9.5
6771.03	Co I	1.88	−1.970	14.7	···	···	···	···	14.6	14.6
6814.94	Co I	1.96	−1.900	···	···	14.2	···	···	12.2	12.2
7417.41	Co I	2.04	−2.070	···	···	···	···	···	10.0	10.0
5578.72	Ni I	1.68	−2.640	54.8	67.2	52.5	41.8	36.5	60.9	60.9
5587.86	Ni I	1.93	−2.140	57.4	56.7	57.6	37.4	34.0	···	···
5592.26	Ni I	1.95	−2.590	61.9	51.4	48.0	···	···	···	···
5748.35	Ni I	1.68	−3.260	···	···	29.4	···	···	21.8	21.8
5846.99	Ni I	1.68	−3.210	23.6	···	···	14.3	···	16.7	16.7
5892.87	Ni I	1.99	−2.340	71.5	64.7	61.0	51.8	35.5	66.6	66.6
6128.97	Ni I	1.68	−3.330	33.8	···	···	11.8	···	26.3	26.3
6176.81	Ni I	4.09	−0.529	···	···	···	···	···	15.0	15.0
6482.80	Ni I	1.93	−2.630	29.5	···	34.3	19.8	24.4	29.4	29.4
6586.31	Ni I	1.95	−2.810	35.8	28.0	30.9	23.9	31.0	35.4	35.4
6643.63	Ni I	1.68	−2.300	102.1	97.4	110.6	88.2	88.0	117.8	117.8
6767.77	Ni I	1.83	−2.170	96.3	97.2	93.3	75.3	66.1	104.6	104.6
6772.31	Ni I	3.66	−0.987	···	···	···	···	···	11.7	11.7
7110.88	Ni I	1.93	−2.970	···	···	···	···	···	28.8	28.8
7122.20	Ni I	3.54	0.048	71.6	61.6	73.9	58.3	53.4	69.5	69.5
7261.92	Ni I	1.95	−2.700	···	···	···	···	···	65.9	65.9
7409.35	Ni I	3.80	−0.100	···	44.8	···	···	···	···	···
7414.50	Ni I	1.99	−2.570	···	54.7	60.6	···	46.0	62.2	62.2
7422.27	Ni I	3.63	−0.129	···	55.0	47.0	···	32.0	47.9	47.9
7574.05	Ni I	3.83	−0.580	···	···	35.8	···	···	16.5	16.5
7727.62	Ni I	3.68	−0.162	···	45.5	44.5	···	···	54.6	54.6
7748.89	Ni I	3.70	−0.130	···	37.6	···	···	42.4	40.5	40.5
7788.93	Ni I	1.95	−2.420	100.7	88.0	87.9	63.9	66.0	92.0	92.0
7797.59	Ni I	3.90	−0.180	···	···	39.5	···	22.3	34.1	34.1
5105.54	Cu I	1.39	−1.505	52.0	61.6	61.9	38.0	39.7	52.8	52.8
5782.12	Cu I	1.64	−1.780	17.5	···	27.2	···	···	18.2	18.2
4722.16	Zn I	4.03	−0.390	27.9	···	39.9	···	···	38.0	38.0
4810.54	Zn I	4.08	−0.170	34.2	···	36.1	···	···	34.0	34.0
4607.33	Sr I	0.00	0.280	28.0	···	11.3	16.0	···	···	···
4215.52	Sr II	0.00	−0.140	240.3	···	···	220.0	···	···	···
4554.04	Ba II	0.00	0.170	···	···	193.4	···	···	···	···
5853.70	Ba II	0.60	−1.010	76.2	84.3	82.4	89.3	95.3	98.9	98.9
6141.70	Ba II	0.70	−0.070	133.4	147.3	138.7	147.2	155.1	187.8	187.8
6496.90	Ba II	0.60	−0.380	137.7	148.6	140.6	155.9	146.4	175.6	175.6
4398.01	Y II	0.13	−1.000	···	···	···	···	···	102.0	102.0
4854.87	Y II	0.99	−0.380	41.7	···	···	48.4	···	···	···
4883.69	Y II	1.08	0.070	68.4	64.0	72.0	66.7	66.0	67.1	67.1
5087.43	Y II	1.08	−0.170	34.0	60.0	44.0	43.2	42.0	49.6	49.6
5123.22	Y II	0.99	−0.830	···	···	33.2	···	···	···	···
5200.42	Y II	0.99	−0.570	42.0	···	···	42.2	···	54.0	54.0
5205.73	Y II	1.03	−0.340	···	···	···	47.0	38.0	···	···
6127.44	Zr I	0.15	−1.060	···	···	···	···	···	6.7	6.7
5122.99	La II	0.32	−0.850	···	···	···	35.2	···	···	···
6390.48	La II	0.32	−1.410	5.1	···	···	···	···	···	···
4486.91	Ce II	0.30	−0.360	24.4	···	···	···	···	···	···
4562.37	Ce II	0.48	0.330	24.3	···	39.1	41.3	···	···	···
4628.16	Ce II	0.52	0.260	30.4	···	26.9	31.6	···	···	···
4462.99	Nd II	0.56	0.040	···	···	···	···	···	27.6	27.6
4959.12	Nd II	0.06	−0.800	25.6	···	36.5	27.4	37.0	32.0	32.0
5092.79	Nd II	0.38	−0.610	···	···	···	···	···	9.9	9.9
5212.35	Nd II	0.20	−0.960	···	···	···	···	···	10.7	10.7
5249.58	Nd II	0.98	0.200	20.3	≤29.0	25.1	23.6	34.2	···	···
4129.70	Eu II	0.00	0.220	98.0	···	132.7	123.8	···	145.0	145.0
6645.11	Eu II	1.38	0.120	11.0	···	12.4	13.4	≤20.0	9.0	9.0